MAX-PLANCK-INSTITUT FÜR PLASMAPHYSIK

GARCHING BEI MÜNCHEN

TRAJECTORIES OF PARTICLES IN A SOLID AND MOMENTS OF DEPTH DISTRIBUTIONS

W. Eckstein

IPP 9/43 October 1983

Die nachstehende Arbeit wurde im Rahmen des Vertrages zwischen dem Max-Planck-Institut für Plasmaphysik und der Europäischen Atomgemeinschaft über die Zusammenarbeit auf dem Gebiete der Plasmaphysik durchgeführt.

W. Eckstein
IPP 9/43
October 1983

Trajectories of Particles in a Solid and Moments of Depth Distributions

Abstract:

Trajectories of H in Ni are shown for five incident energies between 0.1 to 300 keV and for three angles of incidence from normal incidence to an angle of incidence of 80^{o}. In addition the first four moments of the depth distributions of implanted particles are given for H, D, T, ^{3}He, Ne, Ar and Xe in Ni versus the incident energy and angle of incidence. Furthermore the average pathlength and its standard deviation as well as the average number of collisions are shown. The Monte Carlo program TRIM was used to calculate the trajectories and data.

Procedure

The TRIM program /1/ was used to calculate the trajectories of implanted and reflected ions as well as the first four moments of the depth distributions of implanted particles.

For the calculation of the trajectories the Molière potential /2/ was used for the determination of the scattering angle and the elastic energy loss. The inelastic energy loss was calculated from the formula and the constants given in the Anderson-Ziegler tables /3/.

For the evaluation of the moments the version TRSPCR1 (Sputtering version of TRIM) was applied. Here the KR-C potential /4/ was chosen. For the inelastic energy loss of the light ions (H, D, T, ^{3}He) the Andersen-Ziegler tables were taken, the Lindhard-Scharff-formula /5/ was used for the heavier ions.

The choice of a different potential in the calculations of the trajectories is of no importance, because only a small number of trajectories can be plotted and therefore a difference due to another potential will not show up. The two potentials used are only slightly different.

Ion trajectories

Ion trajectories in a solid were first published by Ishitani et al. /6/. They presented trajectories of 30 keV (one at 20 keV) H and D and 300 keV Ne and Kr onto Al, Cu, Au at two angles of incidence. Their main emphasis was laid on the trajectories of the implanted particles. In this report the dependence of the trajectories on the incident energy and incident angle as well as the target mass is shown. One purpose was to demonstrate that rather high energies (several 100 keV for H) are necessary to describe the trajectory of a reflected particle in the solid by straight lines and a single collision. With decreasing

incident energy the correlation between emergent energy and the depth of scattering gets lost. The second purpose was to show that at low energies the average depth where the particles come to rest does not depend on the angle of incidence.

The trajectories shown in the figures 1-15 are projected in a plane normal to the surface. The dashed line indicates the surface. Nickel is bombarded with H. The incident energy, E_o, is varied from 0.1 keV to 300 keV. Three angles of incidence are chosen: $\alpha = 0^o$, 45^o and 80^o (in respect to the surface normal). At one incident energy and incident angle two separate plots have been made: one for those particles which come to rest in the solid (implanted particles) and another one for the reflected particles. For the high energies a large number of incident particles had to be chosen for the reflected particles because of the decreasing particle reflection coefficient. The scales in the plots for the implanted and reflected particles are the same for each incident energy E_o in depth and lateral dimensions for $\alpha = 0^o$ and 45^o. For $\alpha = 80^o$ the scales had to be chosen differently. The dependence of the trajectories on the target mass is shown in Fig. 16 and 17 for the bombardment of C and Au with 10 keV H. In general the single collision model for reflected particles based on straight trajectories before and after a strong collision works at lower energies for H than for heavier incident ions.

Moments of the depth distributions

The figures 18-27 show the dependence of the four moments of the depth distributions of the implanted particles on the incident energy, E_o, and incident angle ,α,. The average depth is the first moment of the depth distributions, the standard deviation of the average depth is the second moment, the skewness

(the unsymmetry of the distribution) is the third moment and the kurtosis (the peakedness of the distribution) is the fourth moment. Indicated in the figures is also the skewness(= 0) and the kurtosis (= 3) for a Gaussian distribution. A positive skewness means a distribution is more shifted to the surface.

In addition, there is given the average pathlength of the implanted particles in the solid and the standard deviation of the pathlength. Also the average number of collisions which a particle needs to come to rest (minimum energy of 5 eV) is shown.

REFERENCES

/1/ J.P. Biersack and L.G. Haggmark
Nucl. Instr. Meth. 174 (1980) 257

/2/ G. Molière, Z. Naturf. A2 (1947) 133

/3/ J. F. Ziegler (editor) Stopping Powers and Ranges in Matter, vol. 3 and 4, Pergamon Press, New York, 1977

/4/ W. Wilson, L. Haggmark and J. Biersack,
Phys. Rev. B 15 (1977) 2458

/5/ J. Lindhard and M. Scharff
Mat.-Fys. Medd, Dan. Vid. Selsk 27 (1953) 15

/6/ T. Ishitani, R. Shimizu and K. Murata
Jap. J. Appl. Phys. 11 (1971) 125.

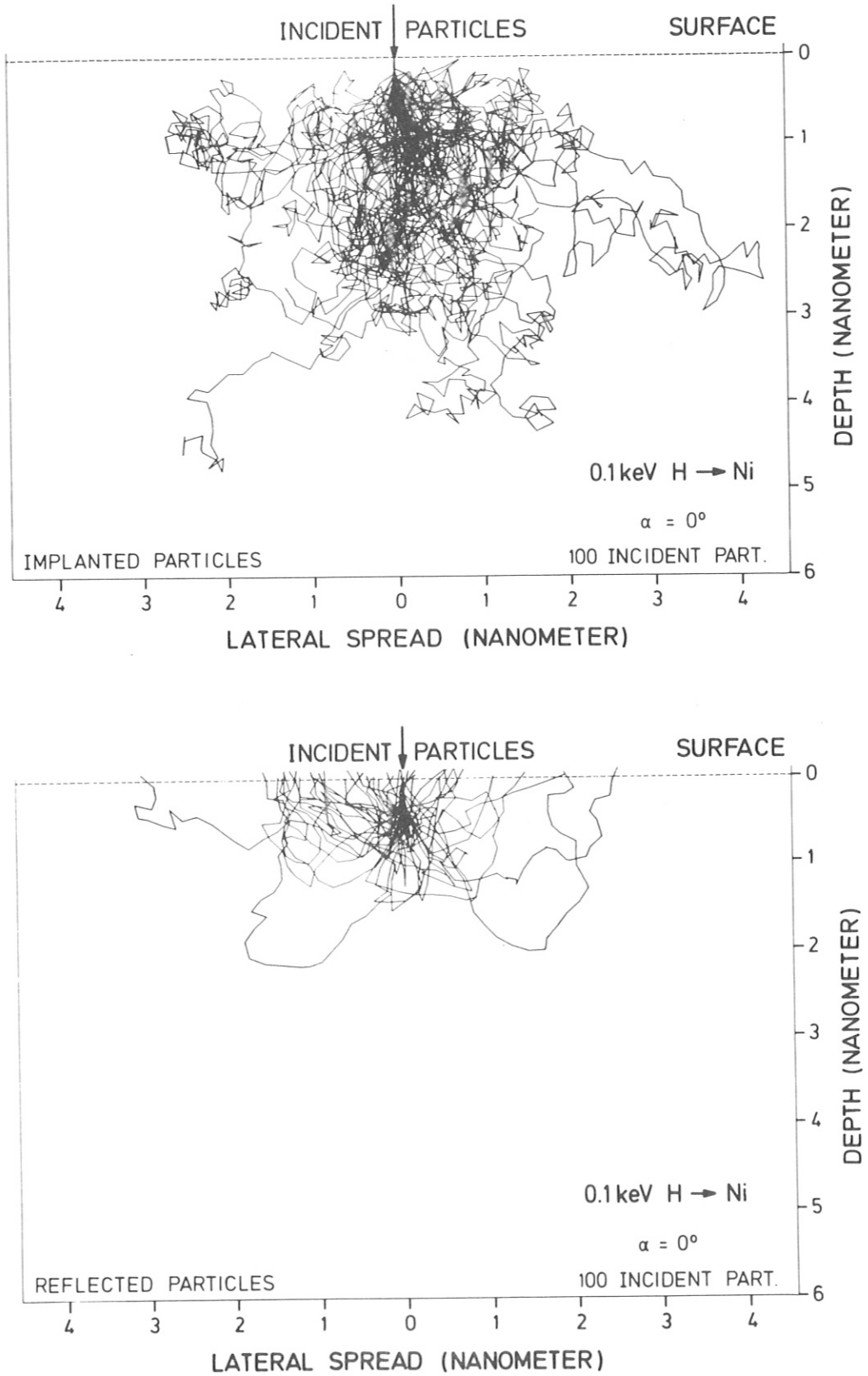

Fig. 1 Bombardment of Ni with 0.1 keV H at normal incidence. The trajectories of the incident particles in the solid are projected onto a plane normal to the surface.
a) implanted particles, b) reflected particles

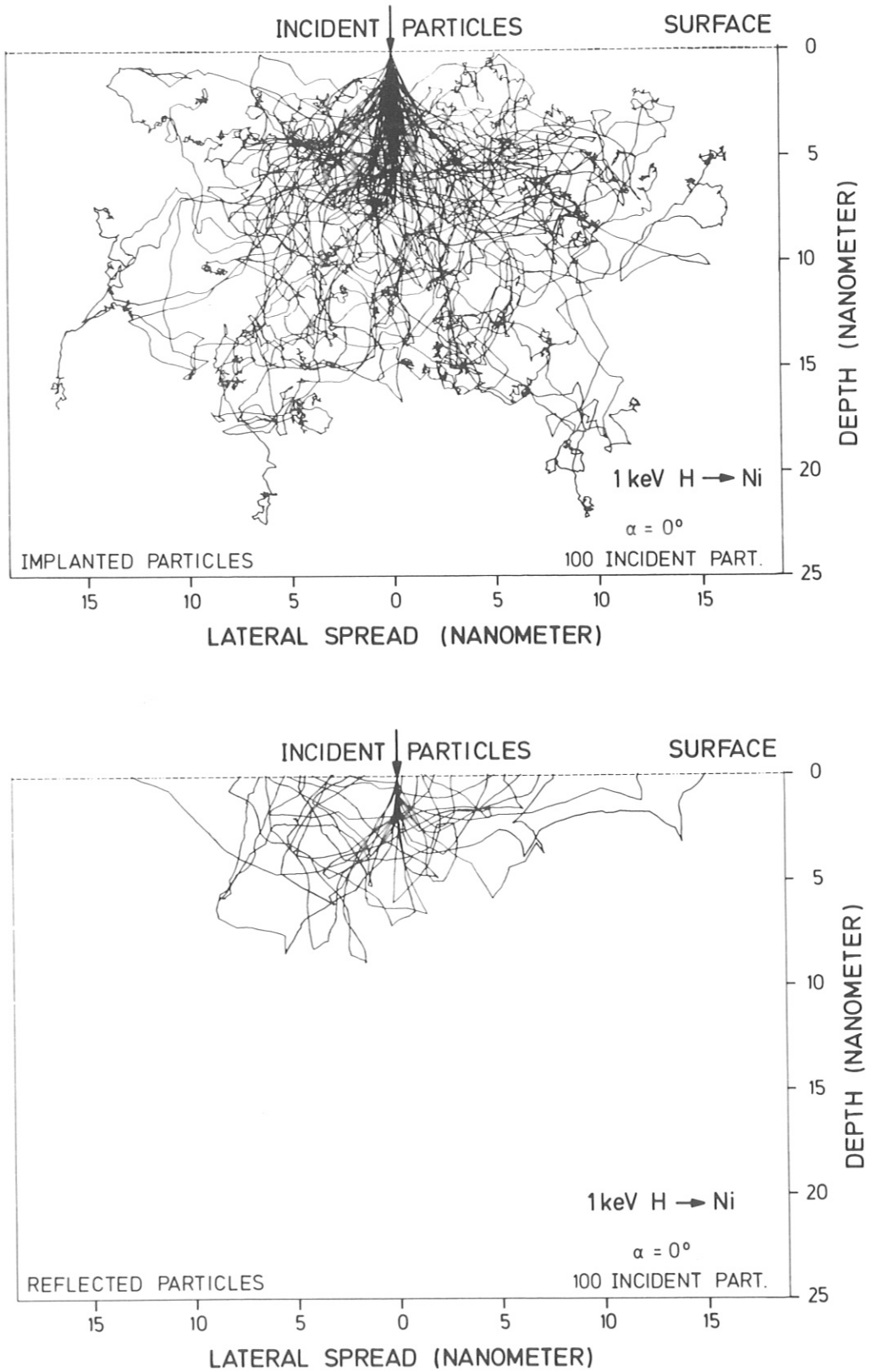

Fig. 2 Bombardment of Ni with 1 keV H at normal incidence: a) implanted particles, b) reflected particles

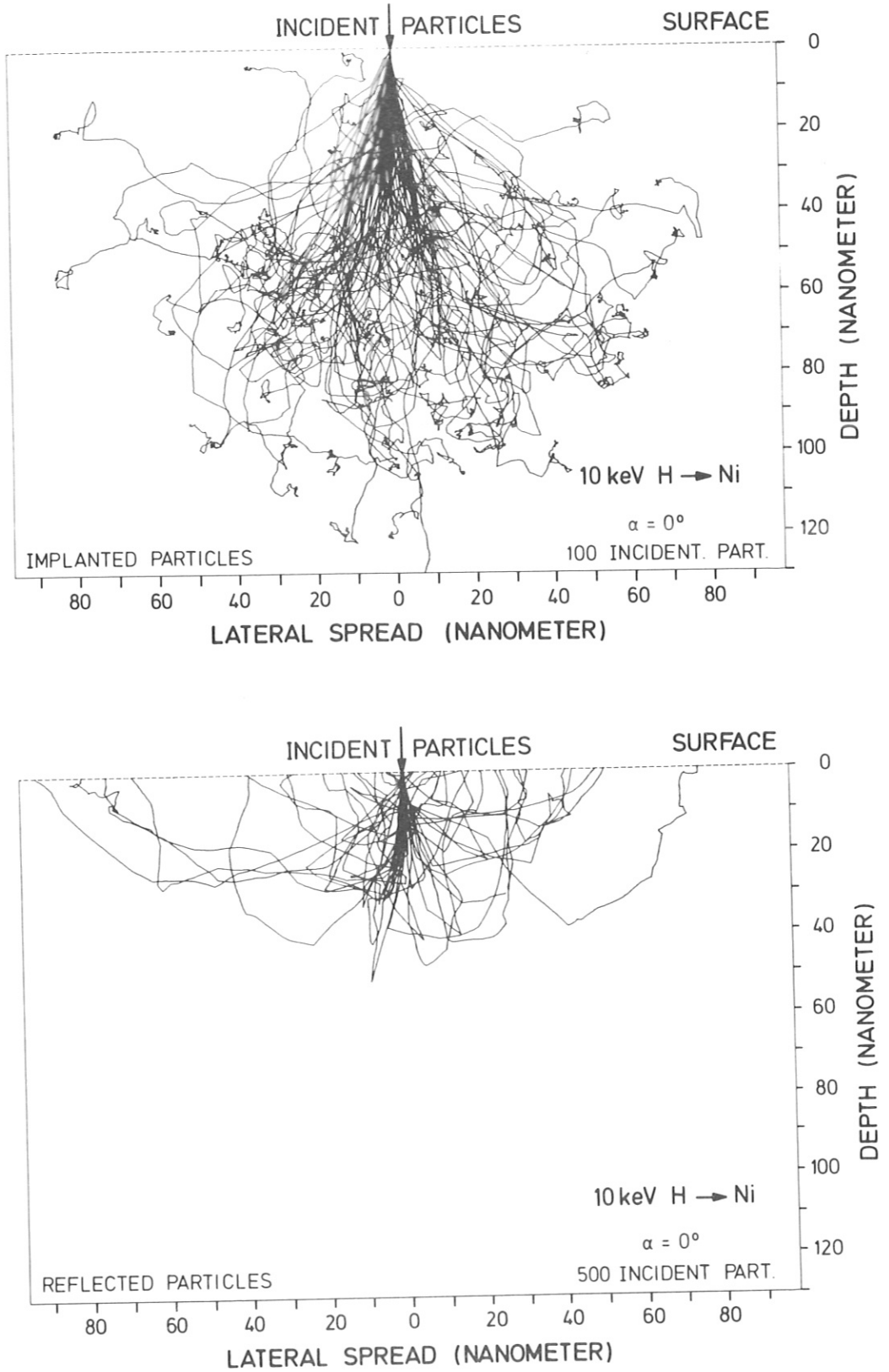

Fig. 3 Bombardment of Ni with 10 keV H at normal incidence: a) implanted particles, b) reflected particles.

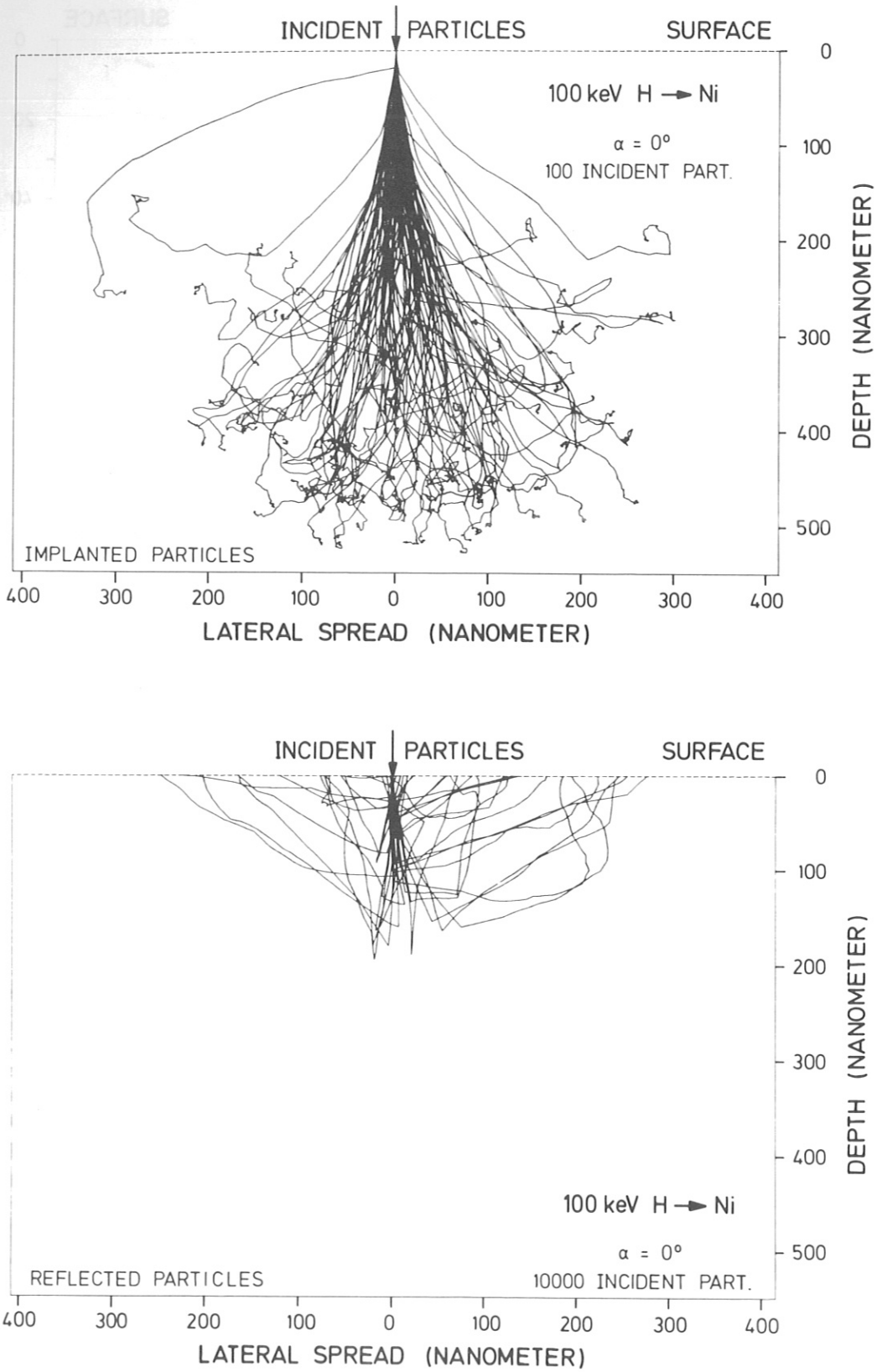

Fig. 4 Bombardment of Ni with 100 keV H at normal incidence: a) implanted particles, b) reflected particles

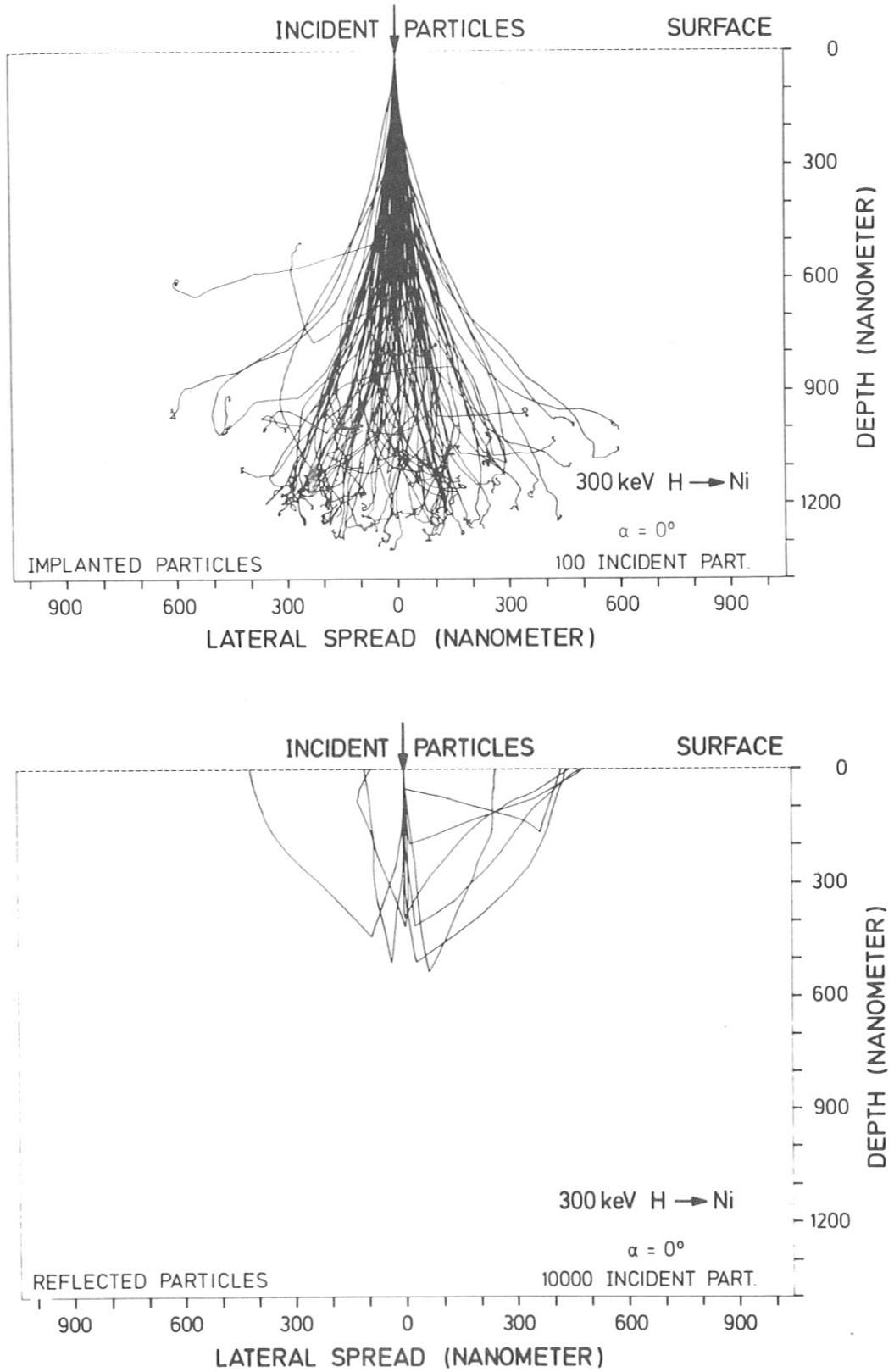

Fig. 5 Bombardment of Ni with 300 keV H at normal incidence: a) implanted particles, b) reflected particles

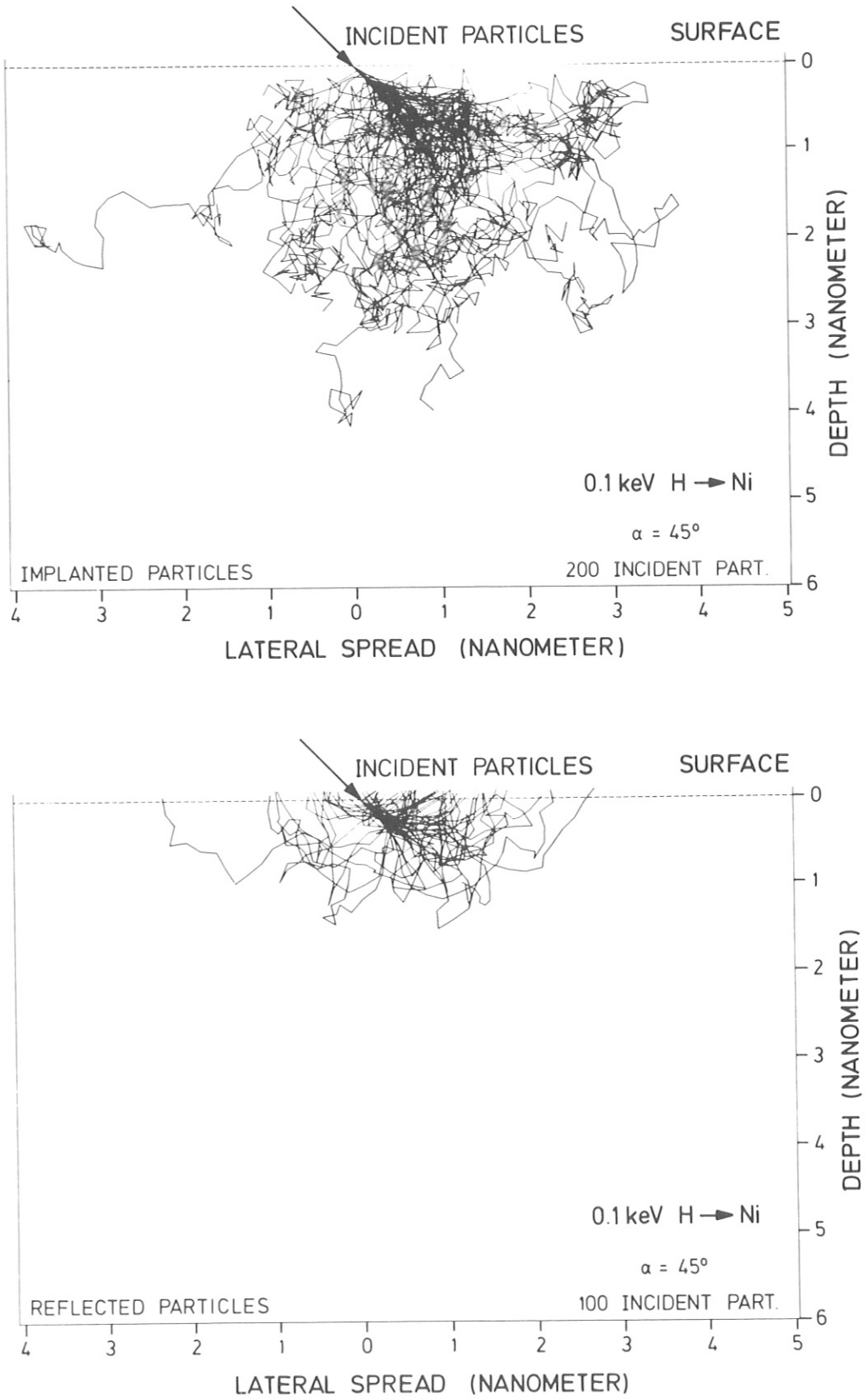

Fig. 6 Bombardment of Ni with 0.1 keV H at an angle of incidence, $\alpha = 45^{o}$:
a) implanted particles, b) reflected particles

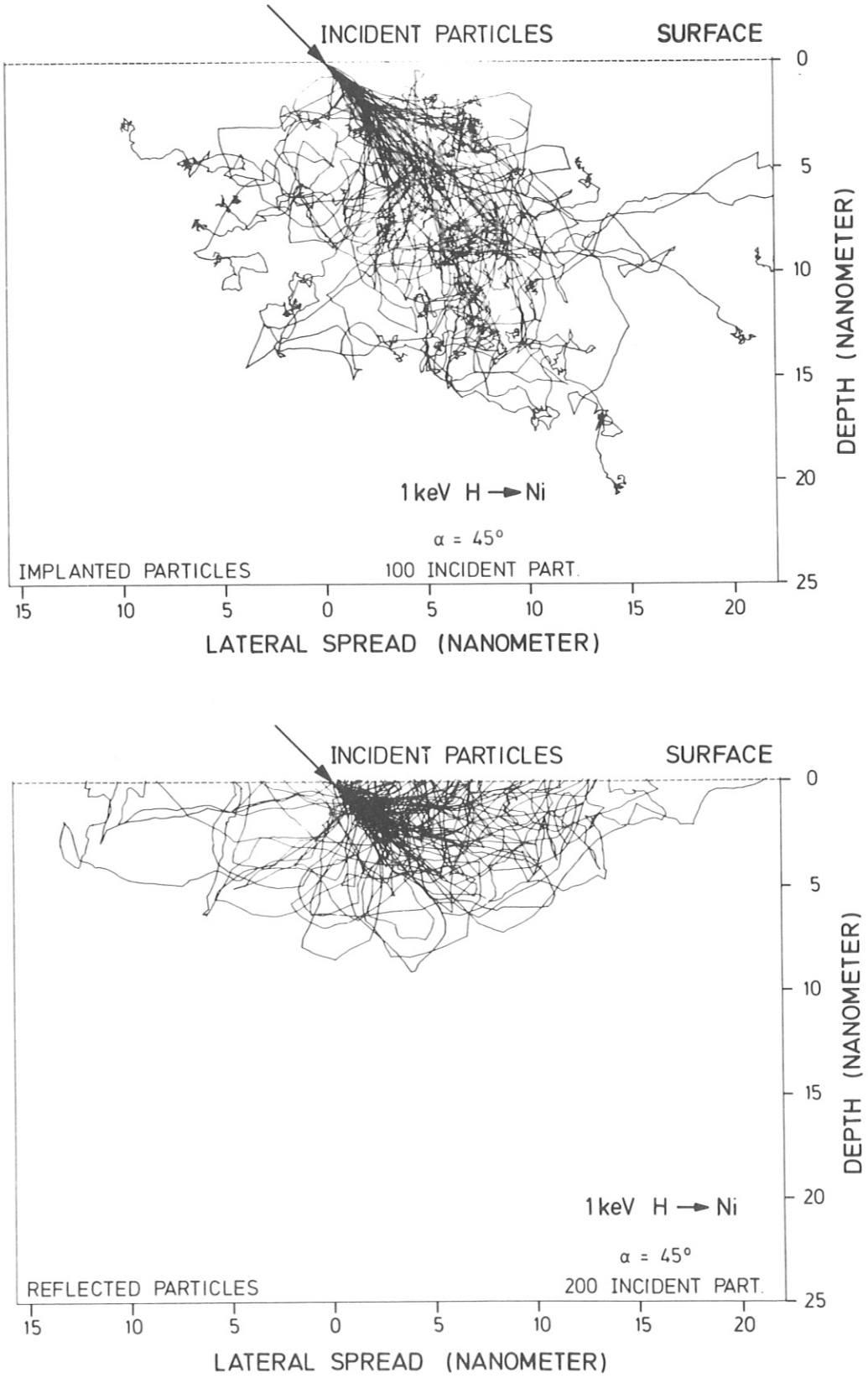

Fig. 7 Bombardment of Ni with 1 keV H at an angle of incidence, $\alpha = 45^{\circ}$:
a) implanted particles, b) reflected particles

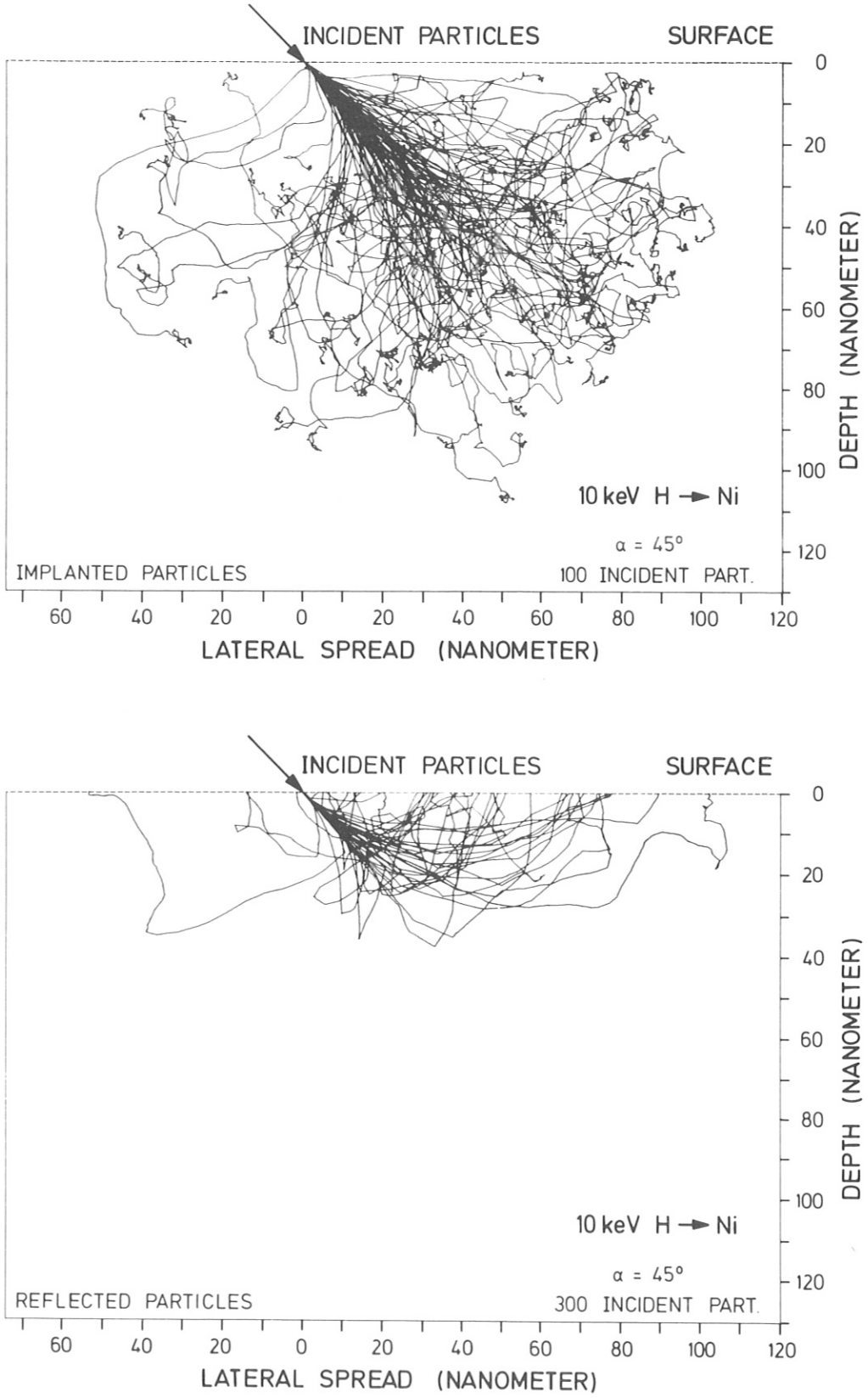

Fig. 8 Bombardment of Ni with 10 keV H at an angle of incidence, $\alpha = 45^{o}$:
a) implanted particles, b) reflected particles

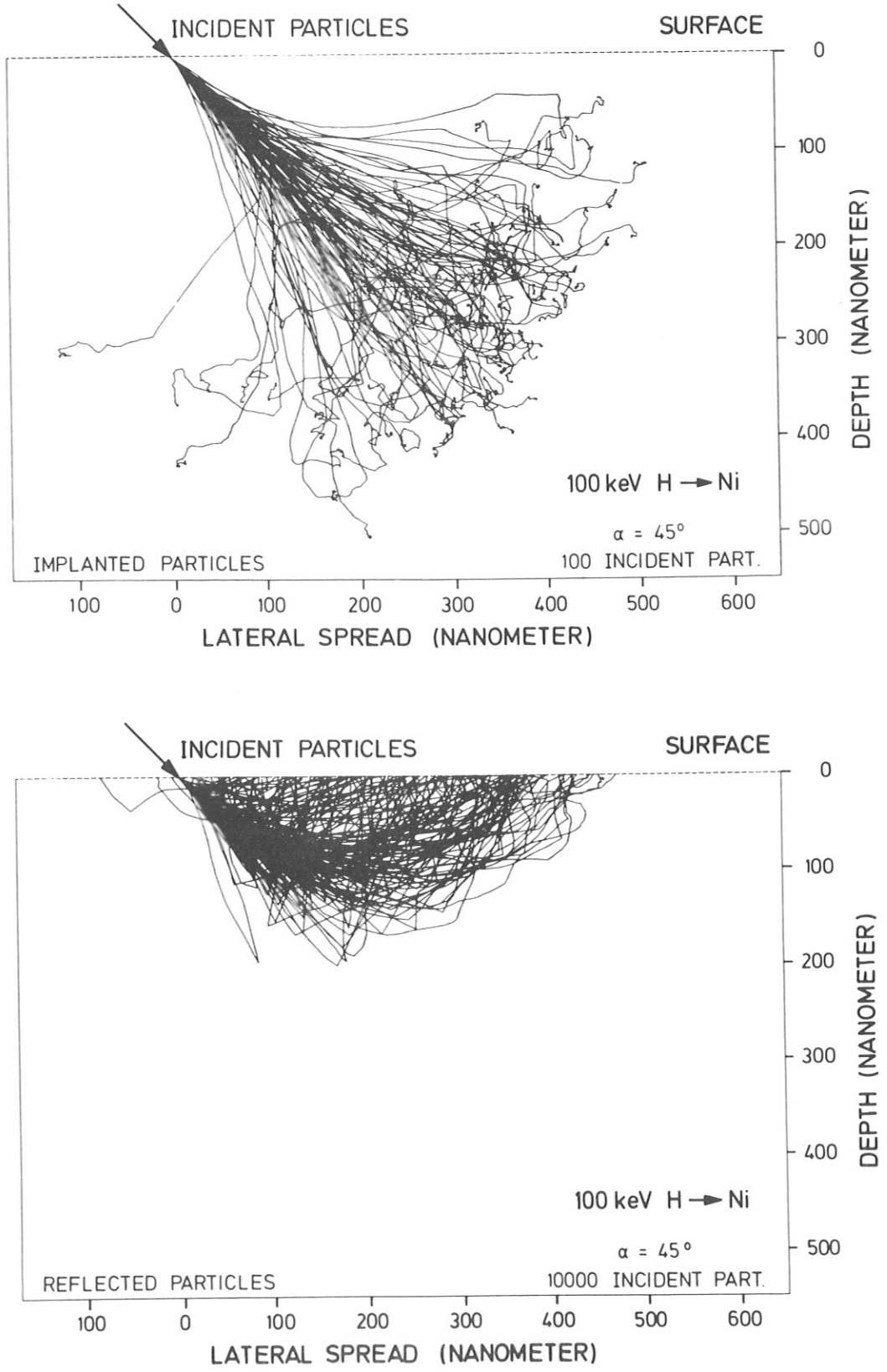

Fig. 9 Bombardment of Ni with 100 keV H at an angle of incidence, $\alpha = 45^{\circ}$:
a) implanted particles, b) reflected particles

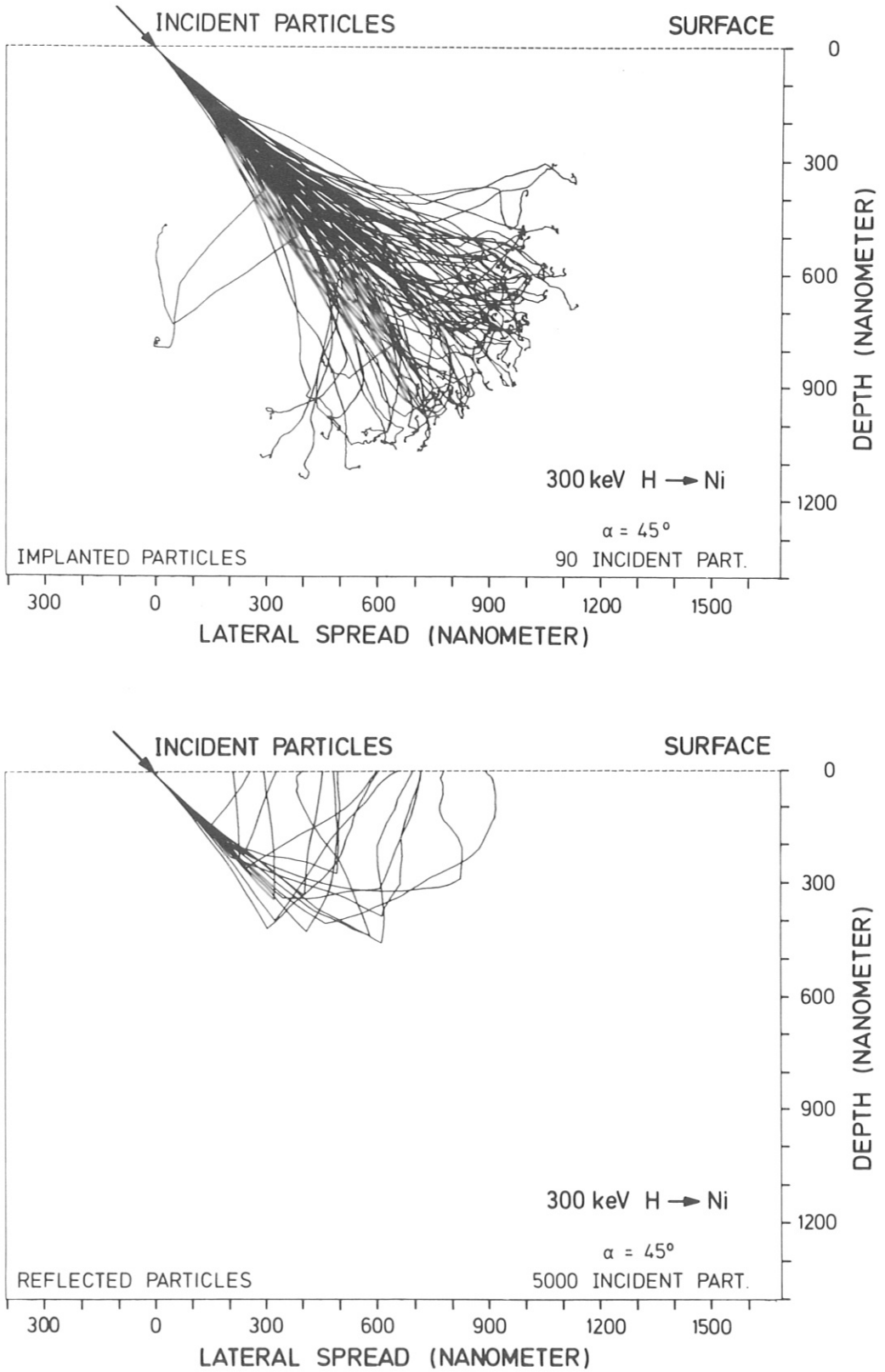

Fig. 10 Bombardment of Ni with 300 keV H at an angle of incidence, $\alpha = 45^{o}$:
a) implanted particles, b) reflected particles

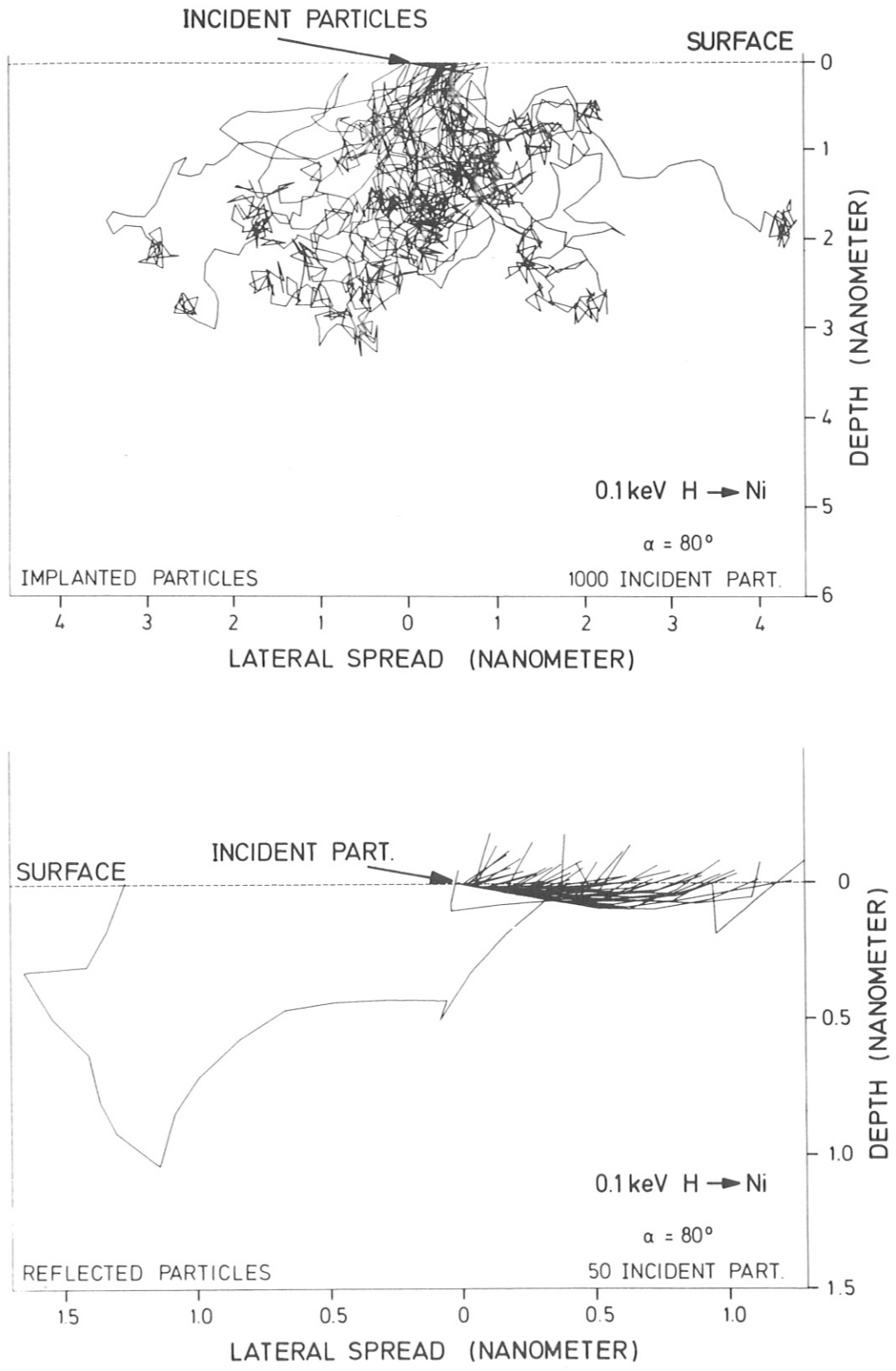

Fig. 11 Bombardment of Ni with 0.1 keV H at an angle of incidence, $\alpha = 80^{o}$:
a) implanted particles, b) reflected particles

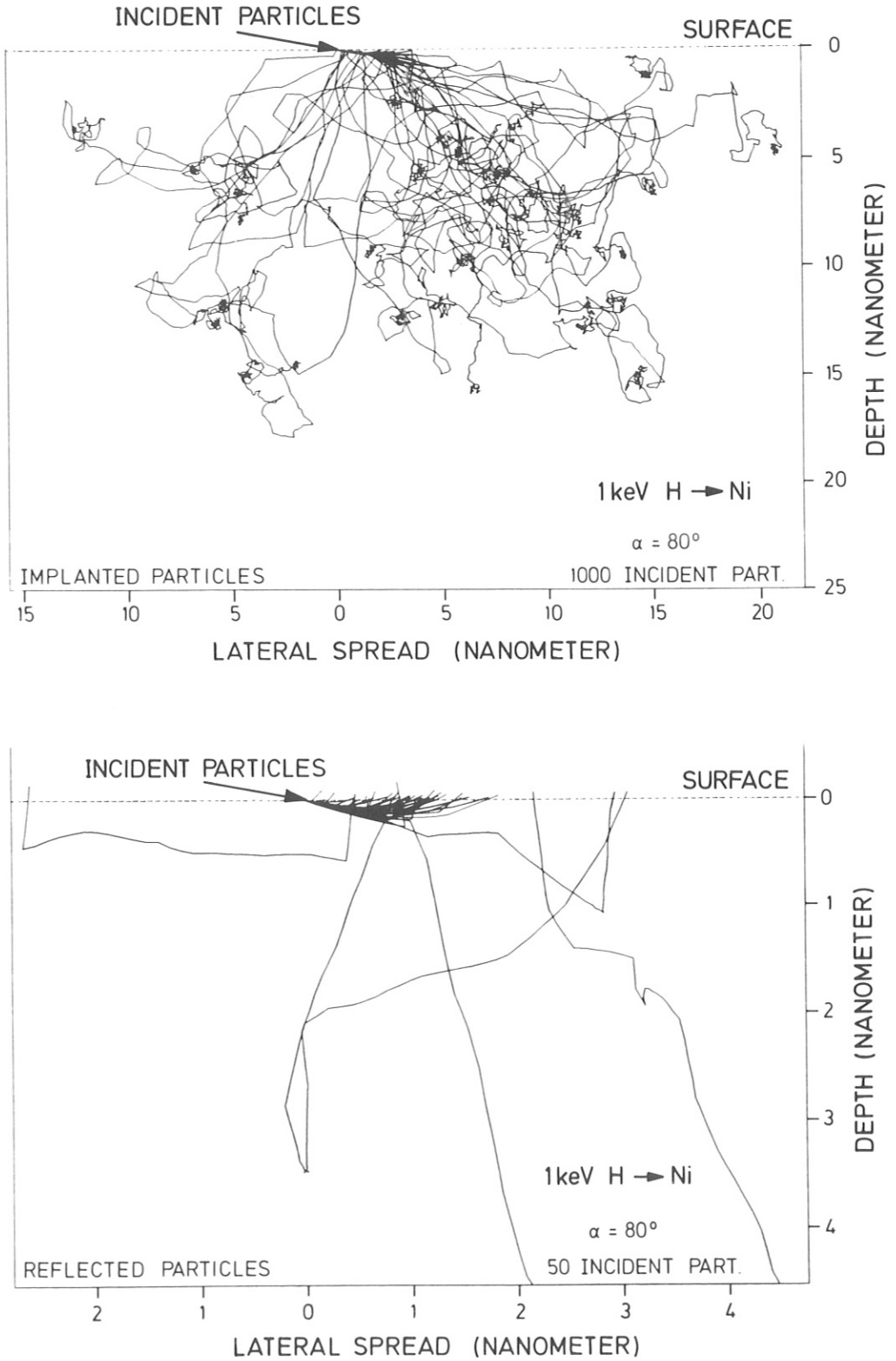

Fig. 12 Bombardment of Ni with 1 keV H at an angle of incidence, $\alpha = 80^{\circ}$:
a) implanted particles, b) reflected particles

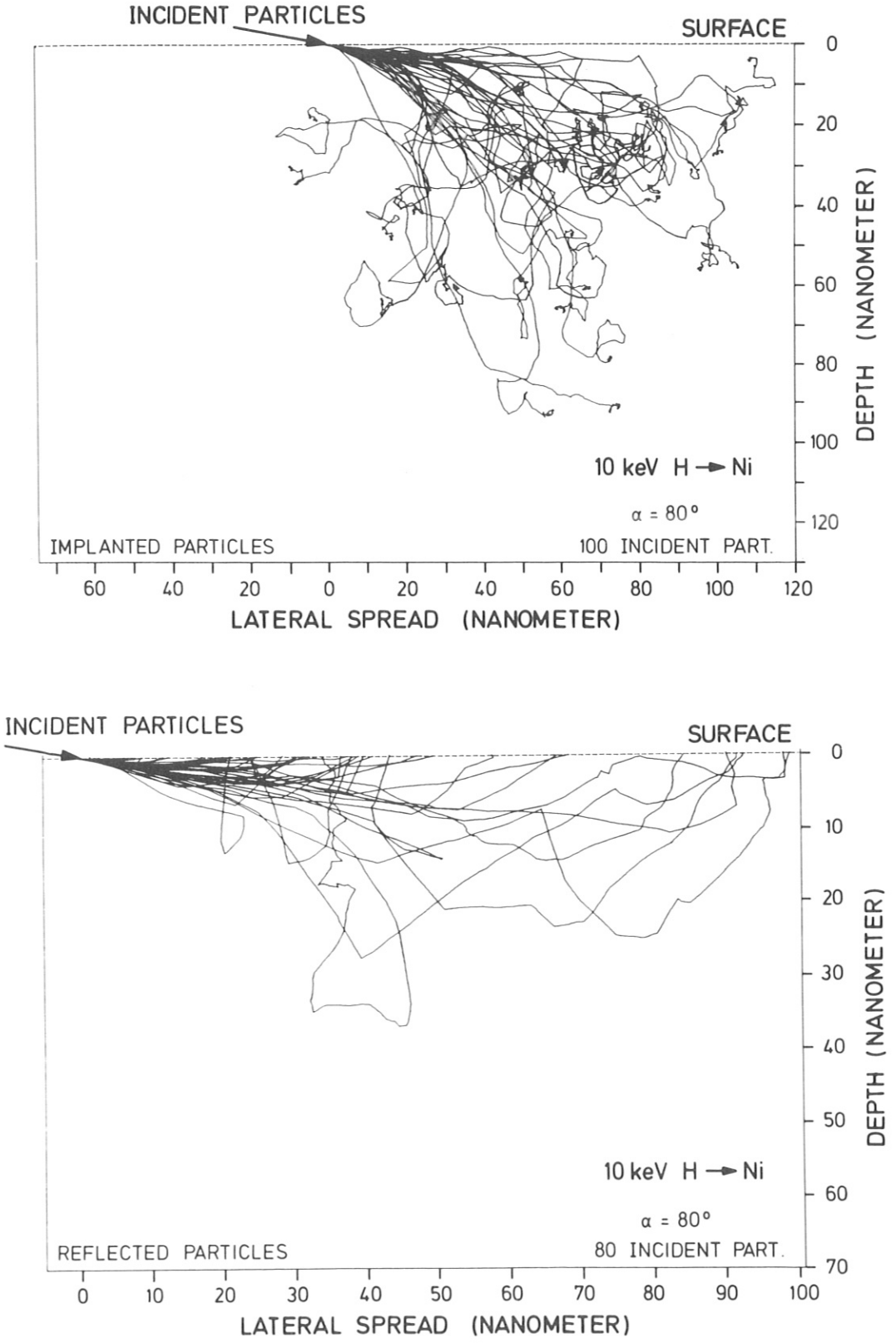

Fig. 13 Bombardment of Ni with 10 keV H at an angle of incidence, $\alpha = 80^{o}$:
a) implanted particles, b) reflected particles

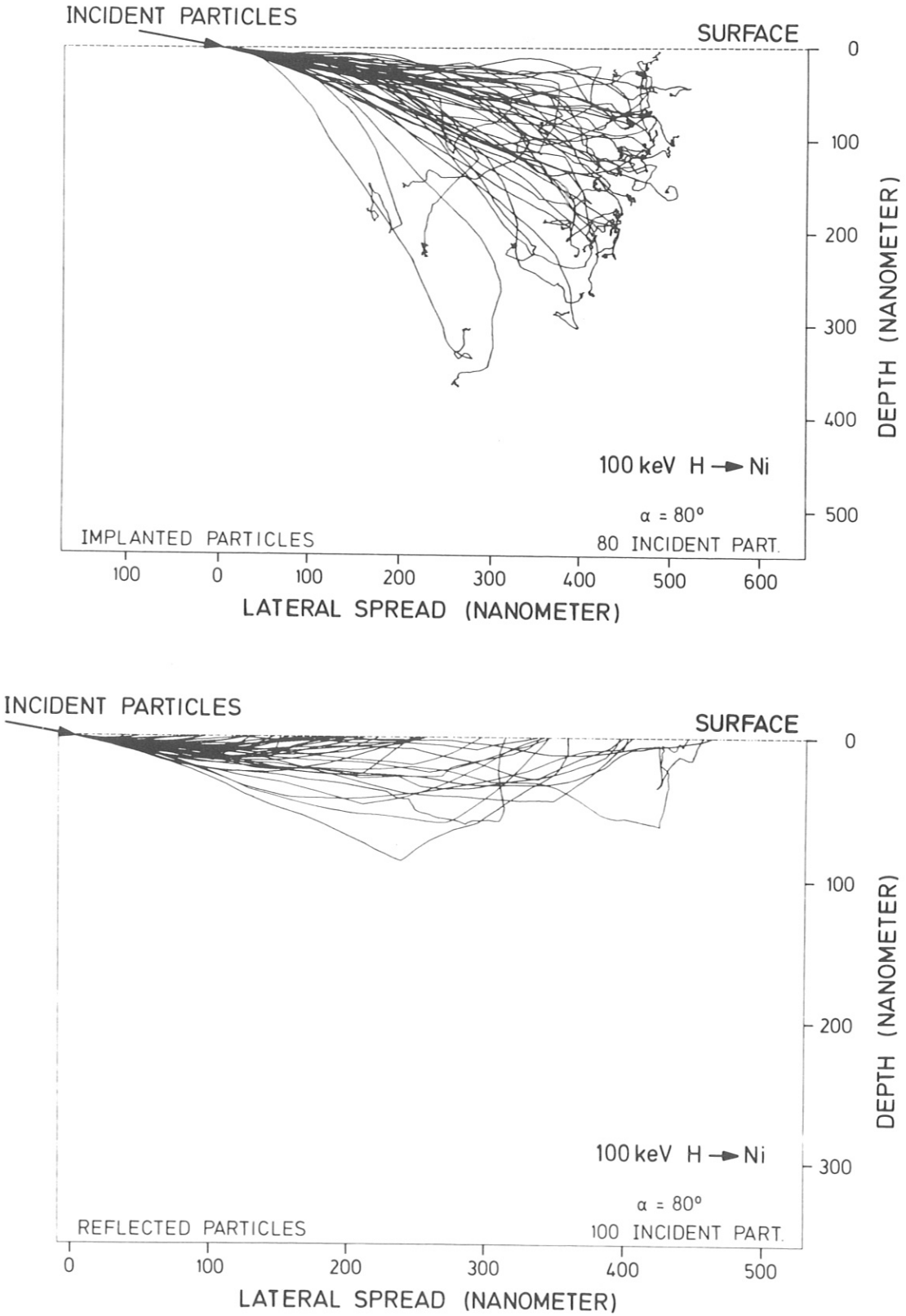

Fig. 14 Bombardment of Ni with 100 keV H at an angle of incidence, $\alpha = 80^{o}$:
a) implanted particles, b) reflected particles

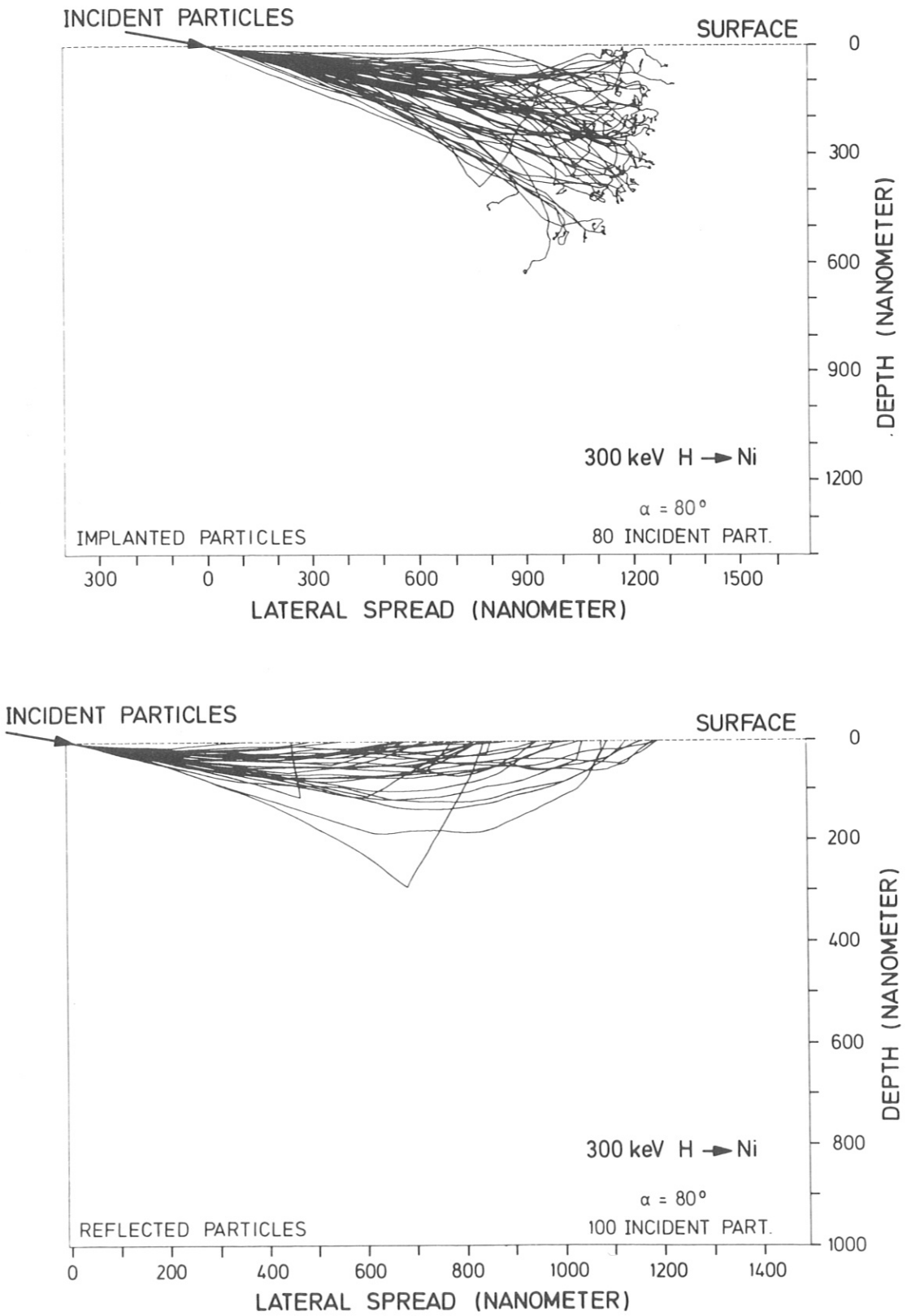

Fig. 15 Bombardment of Ni with 300 keV H at an angle of incidence, $\alpha = 80^{\circ}$:
a) implanted particles, b) reflected particles

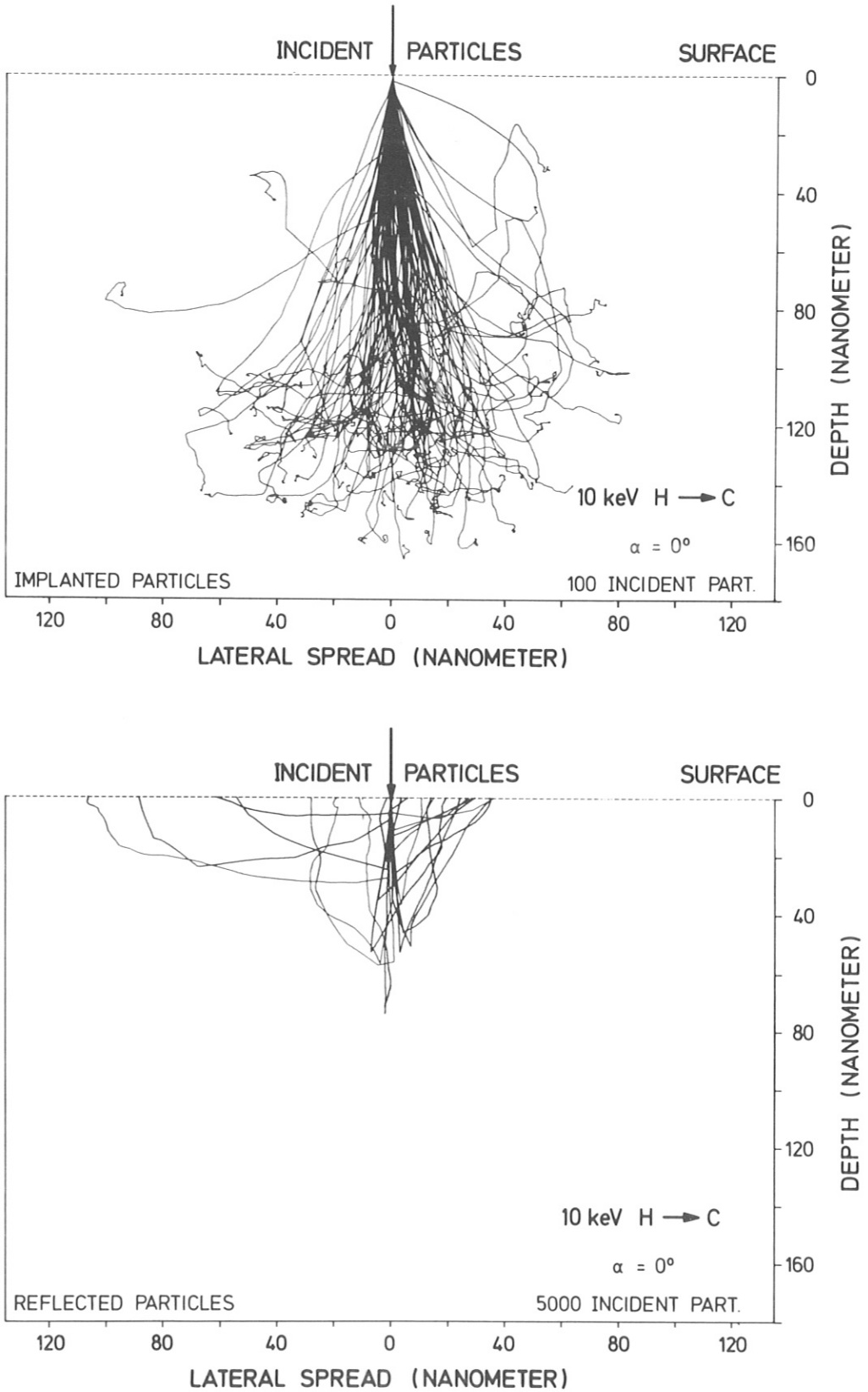

Fig. 16 Bombardment of C with 10 keV H at normal incidence:
a) implanted particles, b) reflected particles

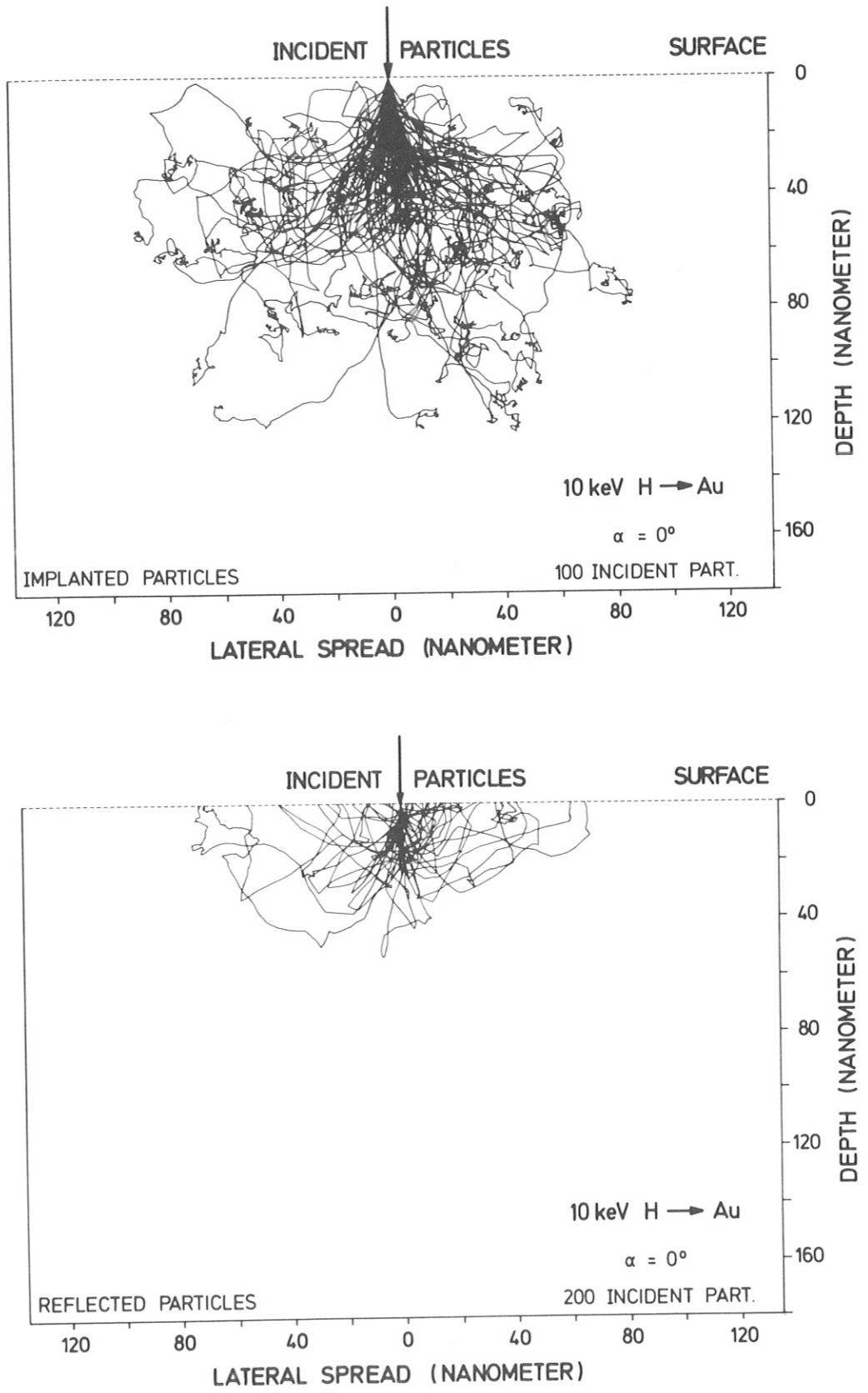

Fig. 17 Bombardment of Au with 10 keV H at normal incidence:
a) implanted particles b) reflected particles

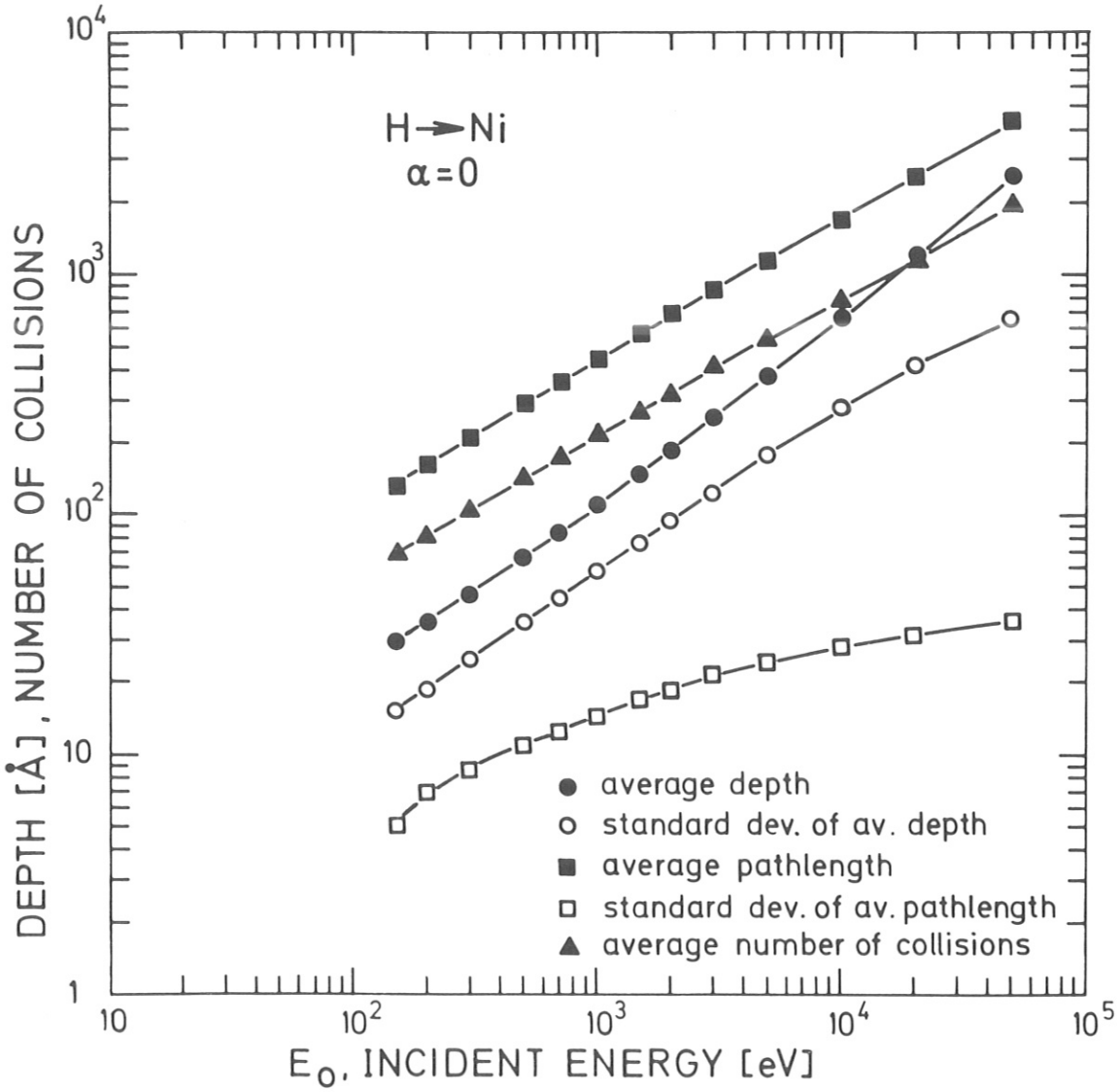

Fig.18a The average depth (mean projected range or 1. moment) and the standard deviation of the average depth (2. moment), the average pathlength and the standard deviation of the average pathlength as well as the average number of collisions are given versus the incident energy, E_o, for the bombardment of Ni with H at normal incidence, $\alpha = 0^o$.

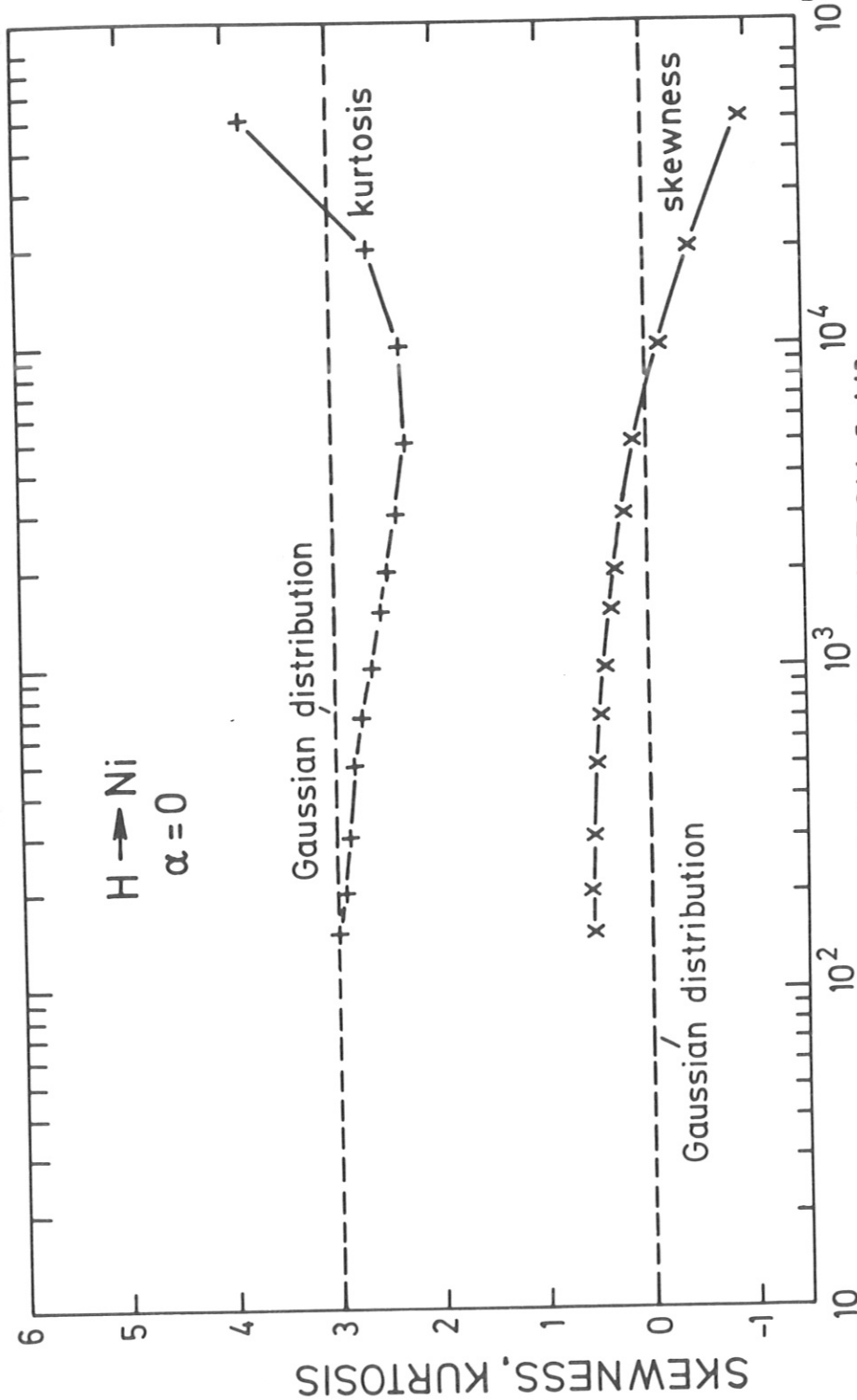

Fig. 18b The skewness (3. moment) and the kurtosis (4. moment of the depth distribution) versus the incidentenergy, E_0, are given for the bombardment of Ni with H at normal incidence.

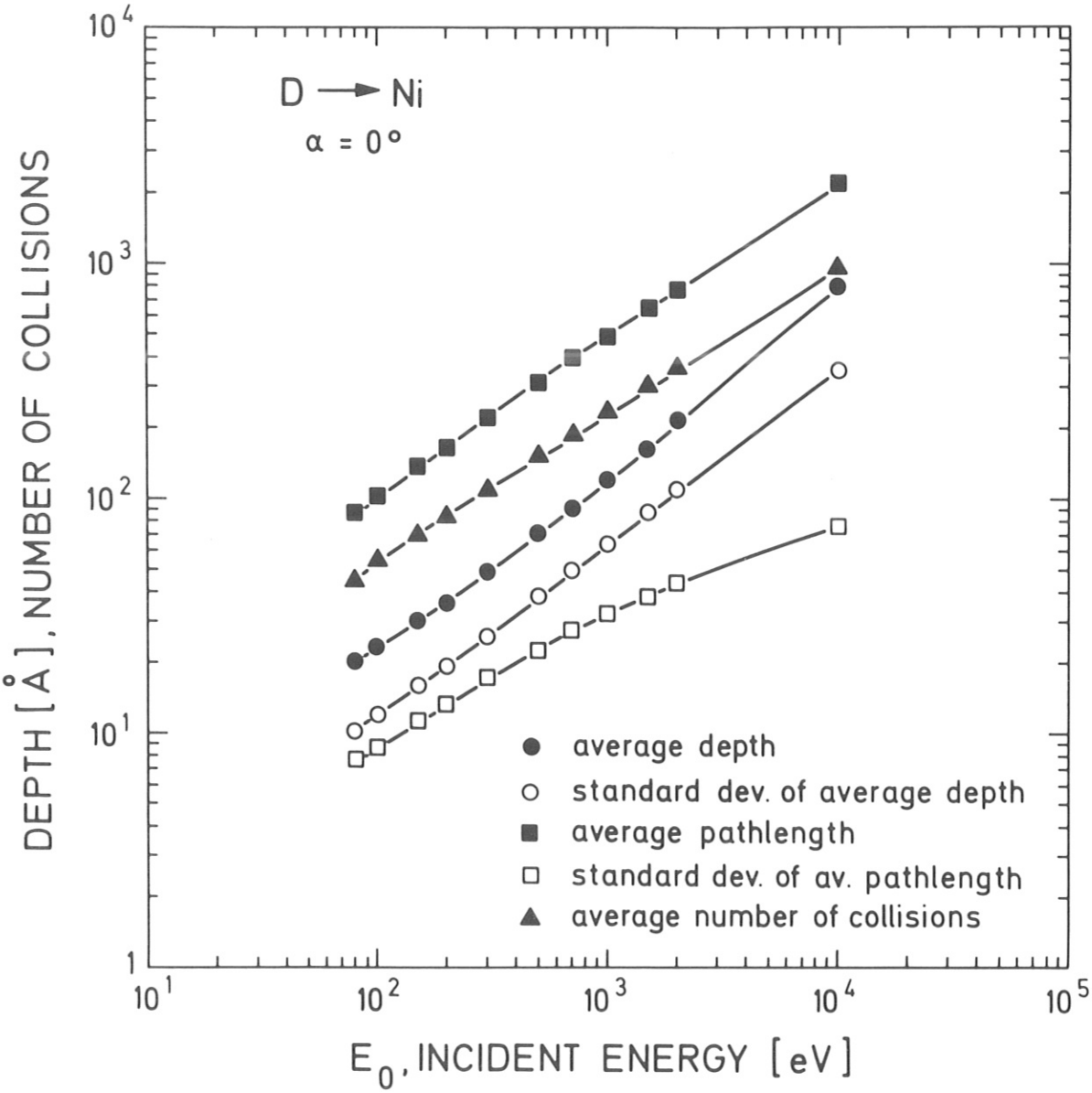

Fig. 19a The average depth (mean projected range or 1.moment) and the standard deviation of the average depth (2. moment), the average pathlength and the standard deviation of the average pathlength as well as the average number of collisions are given versus the incident energy, E_0, for the bombardment of Ni with D at normal incidence, $\alpha = 0^o$.

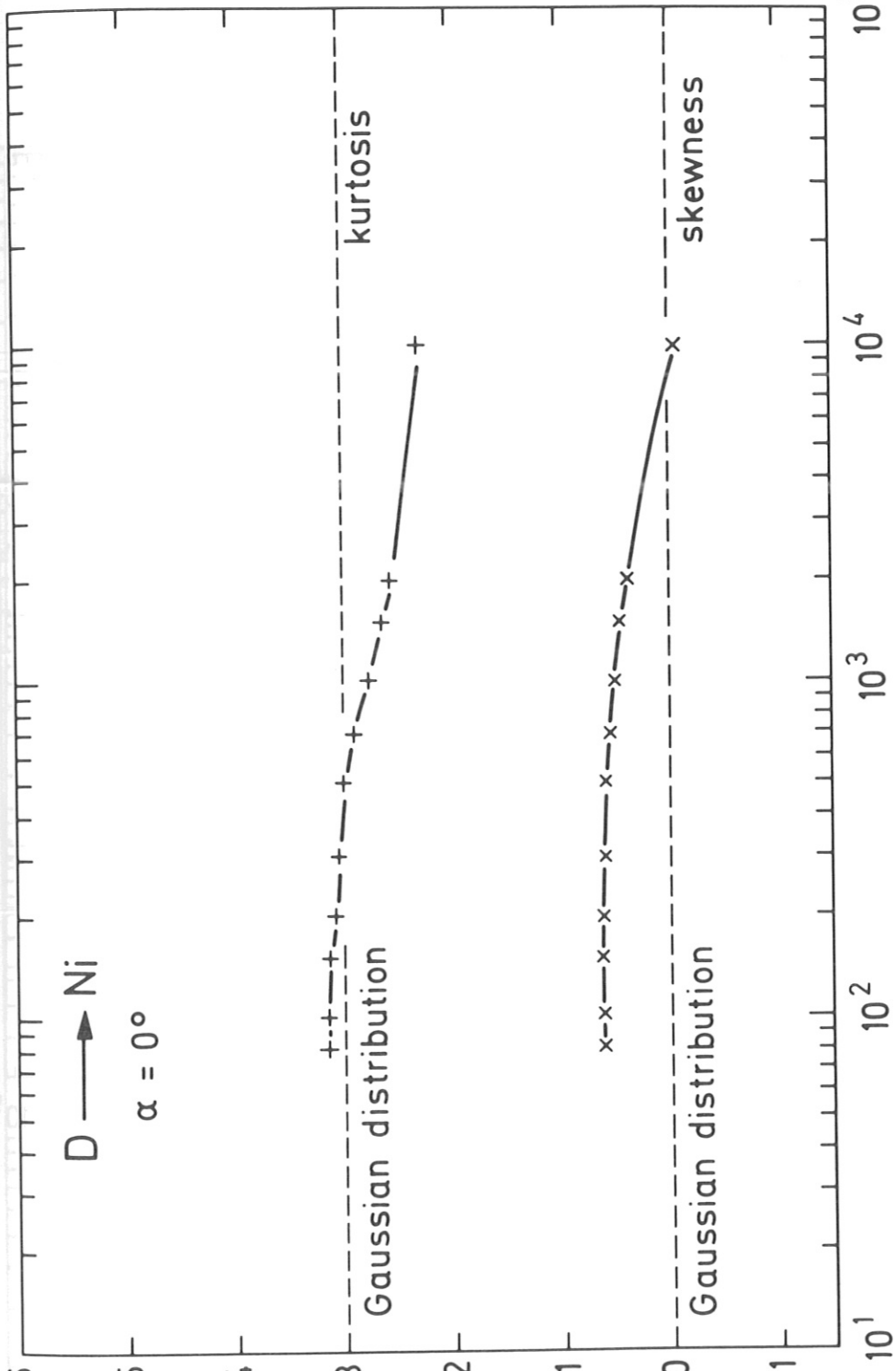

Fig. 19b The skewness (3. moment) and the kurtosis (4. moment of the depth distribution) versus the incident energy, E_o, are given for the bombardment of Ni with D at normal incidence.

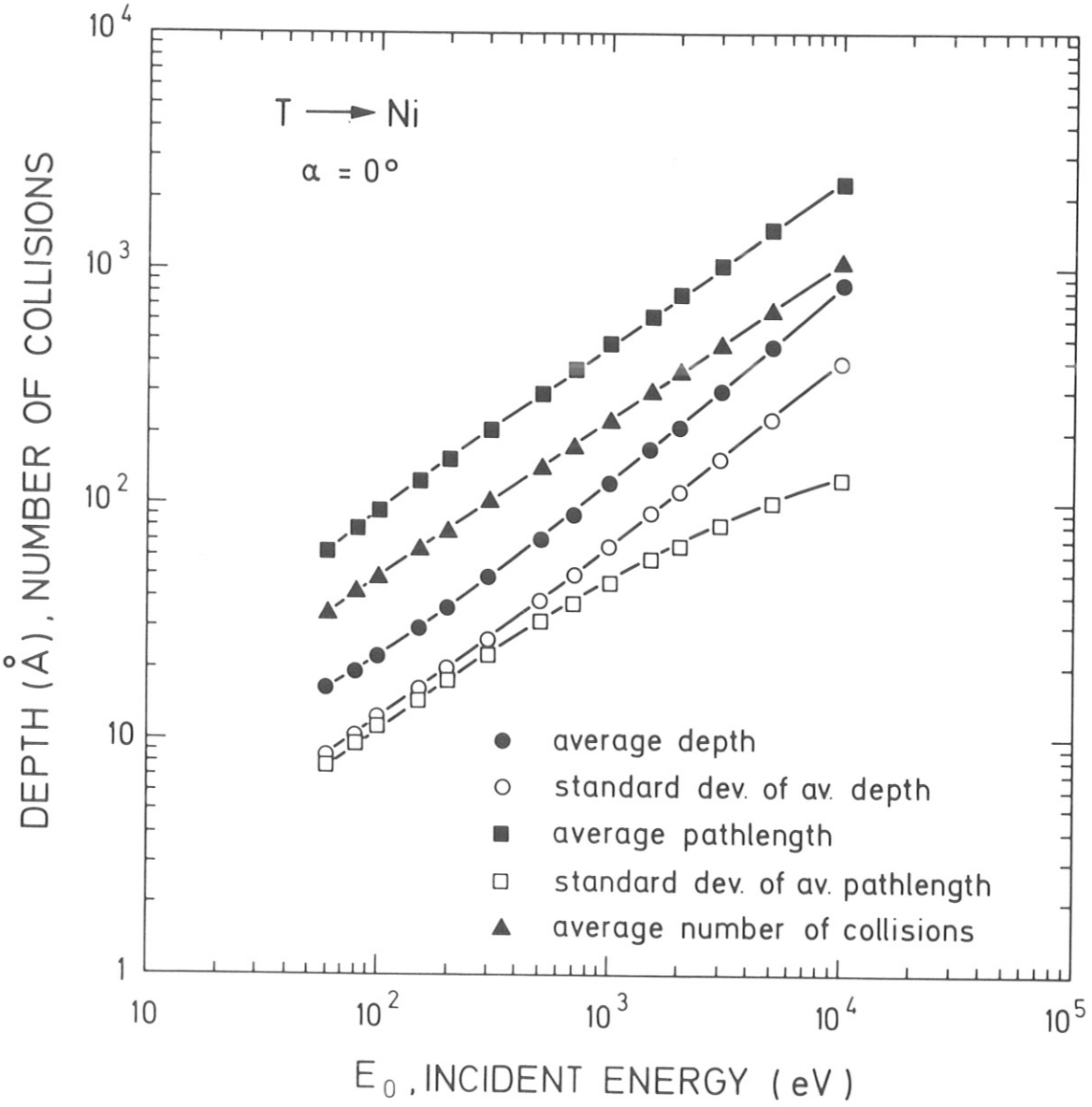

Fig. 20a The average depth (mean projected range or 1. moment) and the standard deviation of the average depth (2. moment), the average pathlength and the standard deviation of the average pathlength as well as the average number of collisions are given versus the incident energy, E_o, for the bombardment of Ni with T at normal incidence, $\alpha = 0^o$.

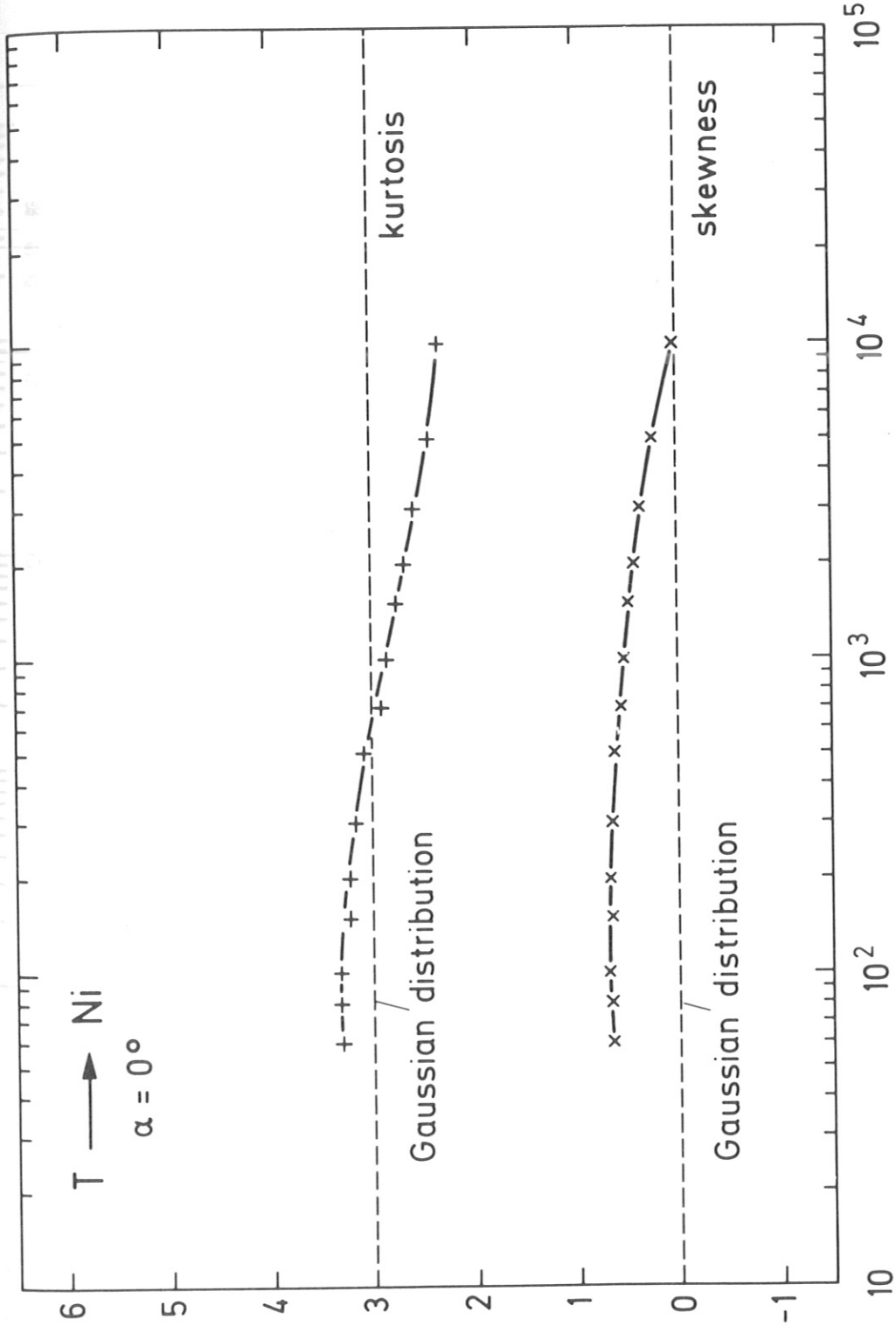

Fig. 20b The skewness (3. moment) and the kurtosis (4.moment of the depth distribution) versus the incident energy, E_o, are given for the bombardment of Ni with T at normal incidence.

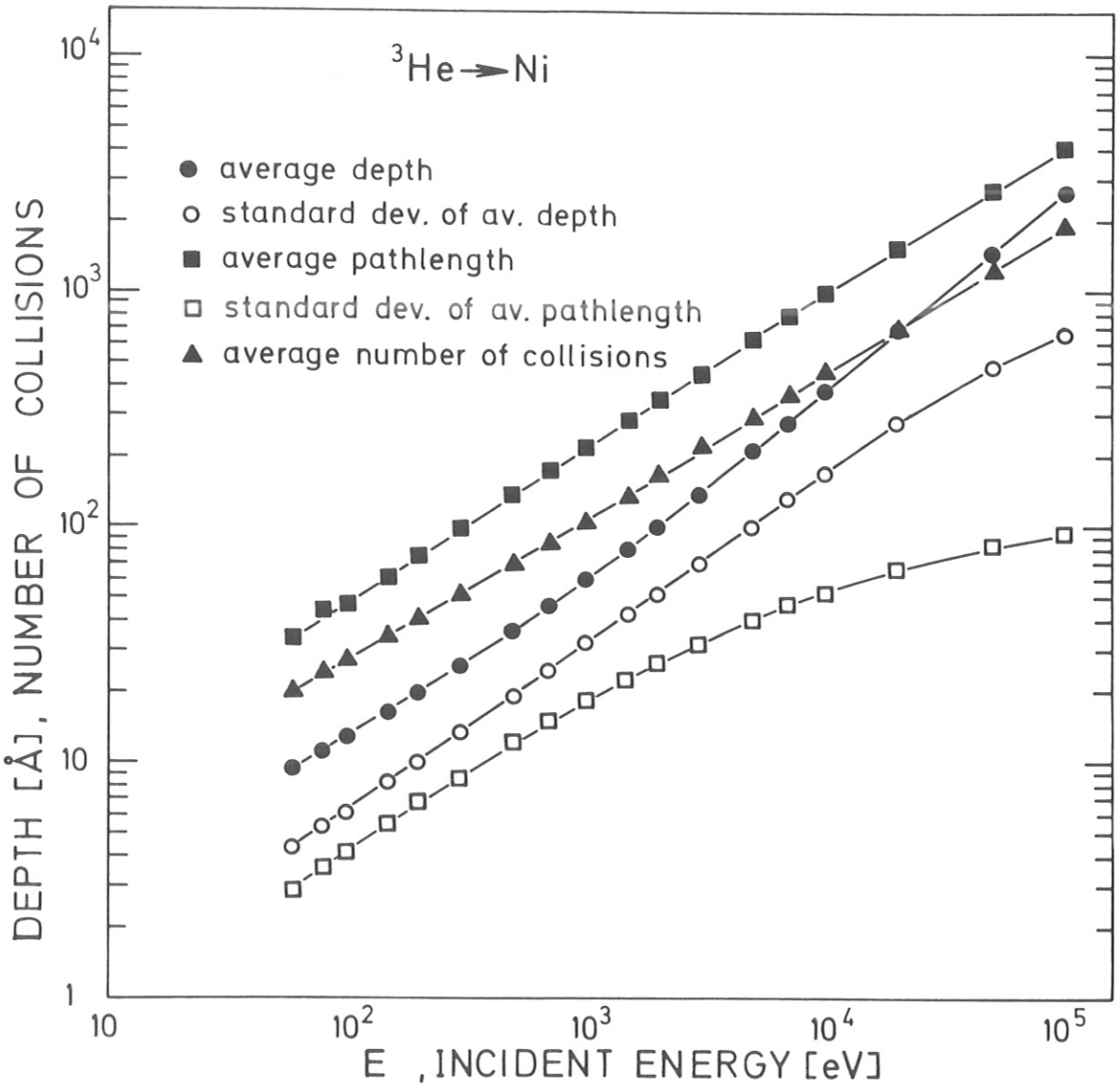

Fig. 21a The average depth (mean projected range or 1. moment) and the standard deviation of the average depth (2. moment), the average pathlength and the standard deviation of the average pathlength as well as the average number of collisions are given versus the incident energy, E_o, for the bombardment of Ni with ^{3}He at normal incidence, $\alpha = 0^o$.

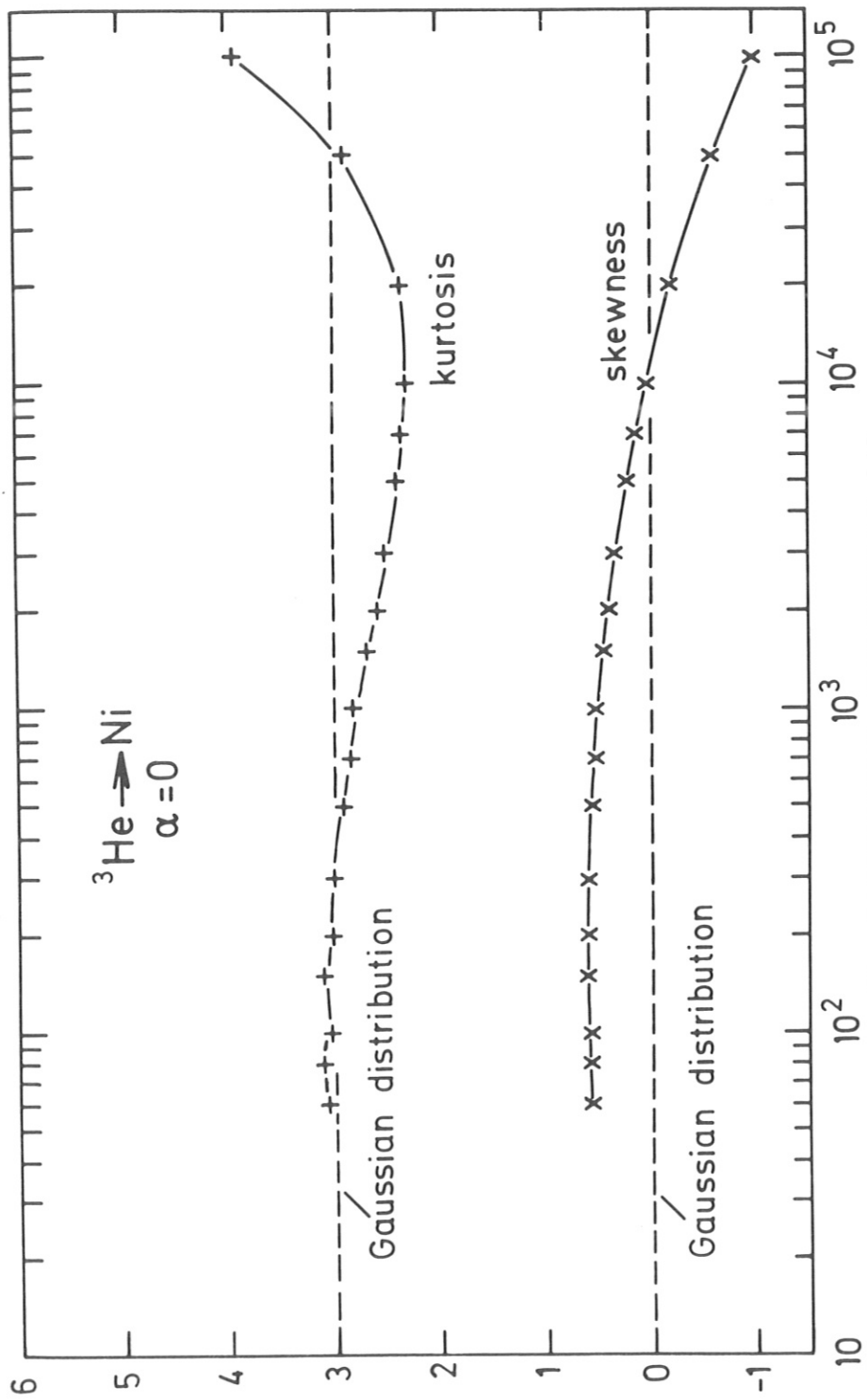

Fig. 21b The skewness (3. moment) and the kurtosis (4. moment of the depth distribution) versus the incident energy, E_0, are given for the bombardment of Ni with ^{3}He at normal incidence.

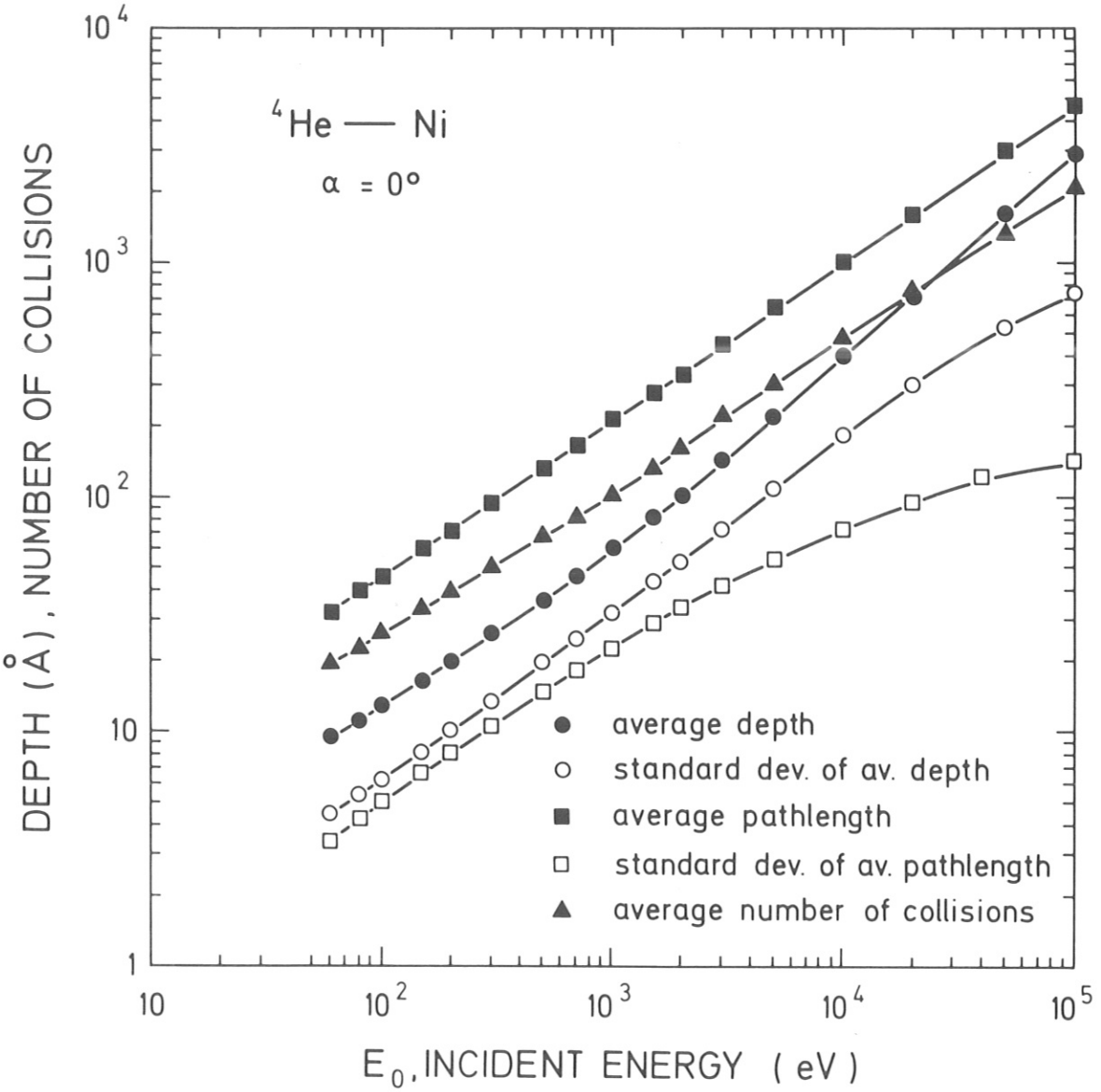

Fig. 22a The average depth (mean projected range or 1. moment) and the standard deviation of the average depth (2. moment), the average pathlength and the standard deviation of the average pathlength as well as the average number of collisions are given versus the incident energy, E_0, for the bombardment of Ni with ^{4}He at normal incidence, $\alpha = 0^o$.

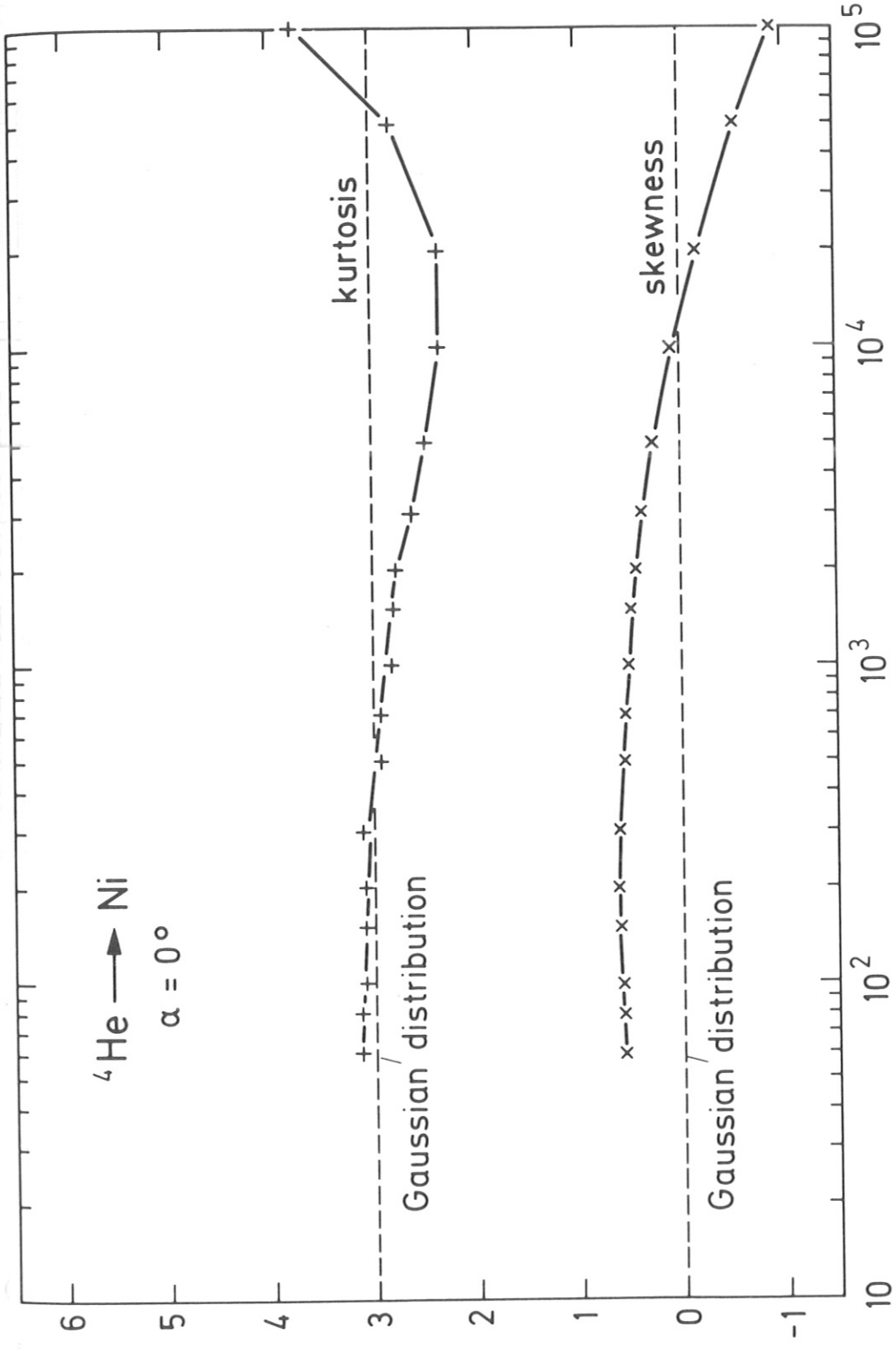

Fig. 22b The skewness (3. moment) and the kurtosis (4. moment of the depth distribution) versus the incident energy, E_0, are given for the bombardment of Ni with ^{4}He at normal incidence.

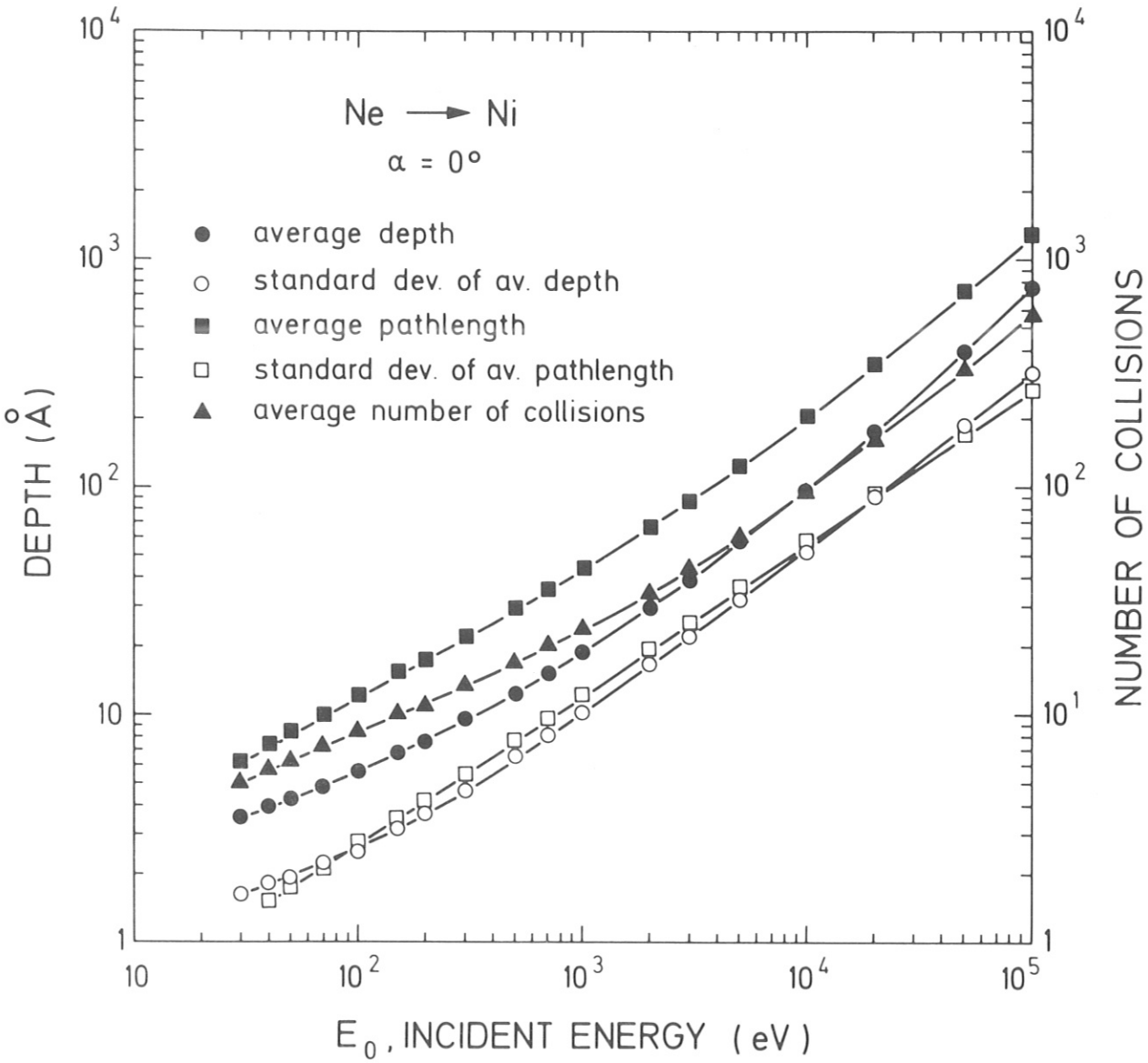

Fig. 23a The average depth (mean projected range or 1. moment) and the standard deviation of the average depth (2. moment), the average pathlength and the standard deviation of the average pathlength as well as the average number of collisions are given versus the incident energy, E_o, for the bombardment of Ni with Ne at normal incidence, $\alpha = 0^o$.

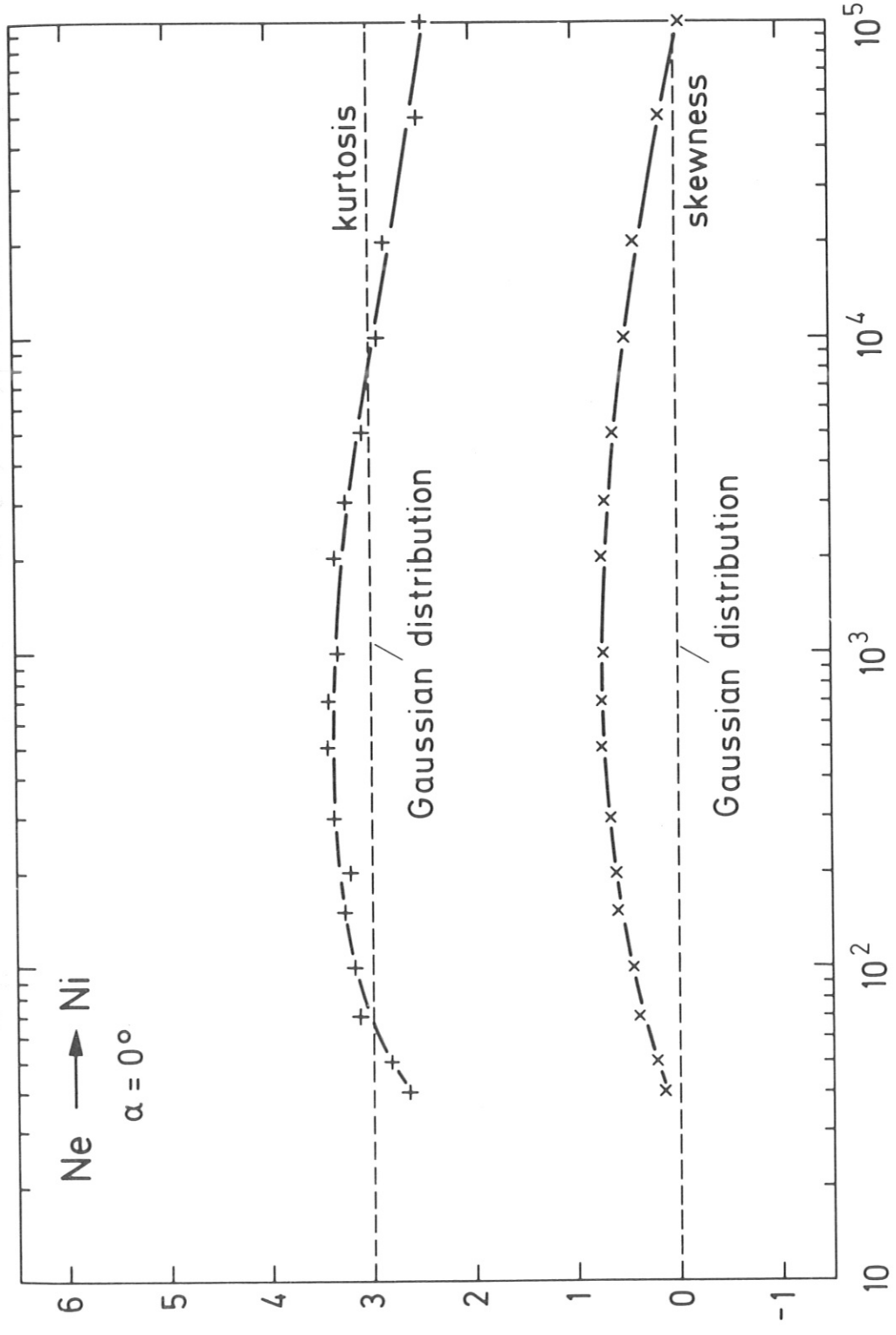

Fig. 23b The skewness (3.moment) and the kurtosis (4. moment of the depth distribution) versus the incident energy, E_0, are given for the bombardment of Ni with Ne at normal incidence.

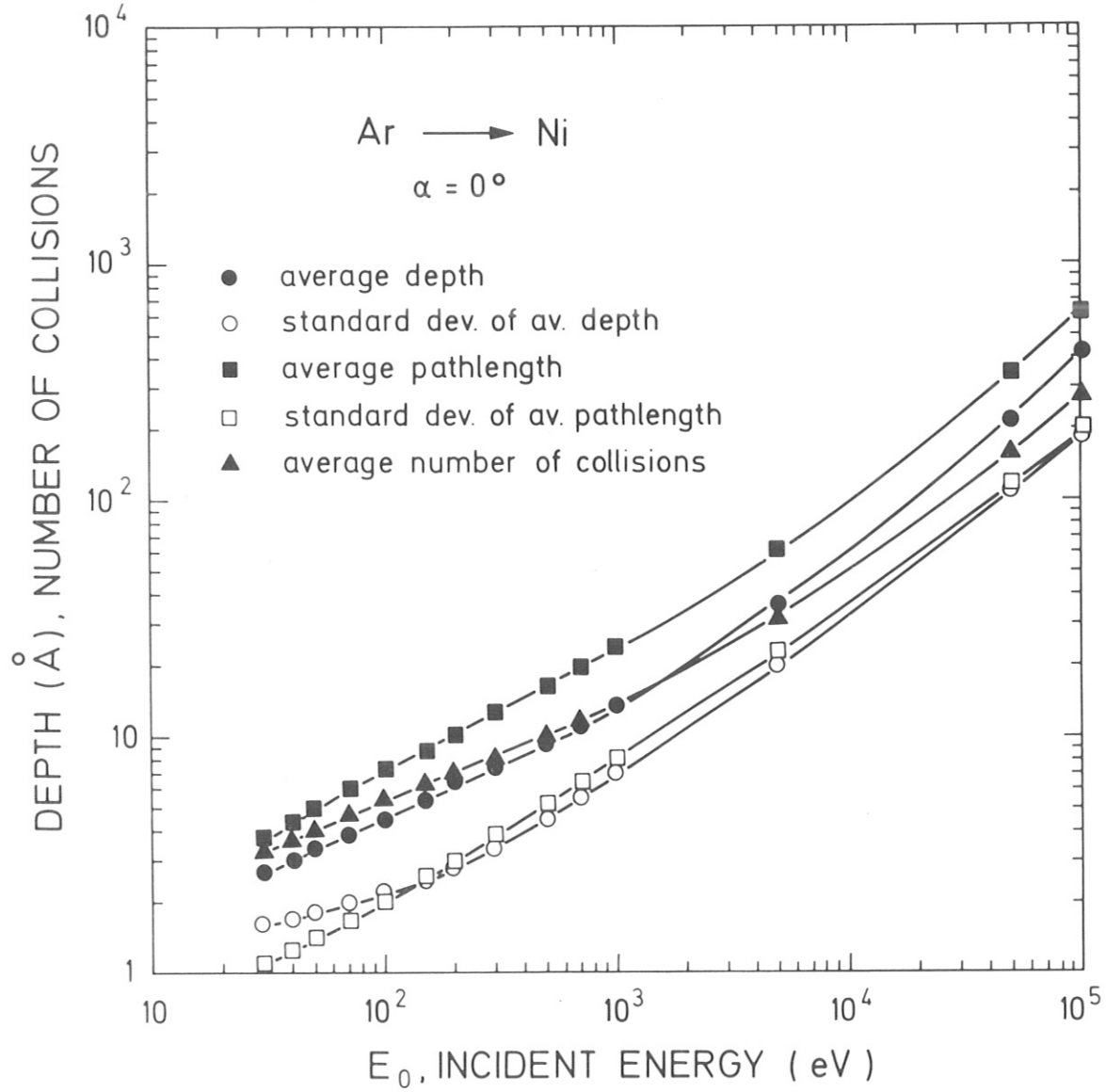

Fig. 24a The average depth (mean projected range or 1. moment) and the standard deviation of the average depth (2. moment), the average pathlength and the standard deviation of the average pathlength as well as the average number of collisions are given versus the incident energy, E_o, for the bombardment of Ni with Ar at normal incidence, $\alpha = 0^o$.

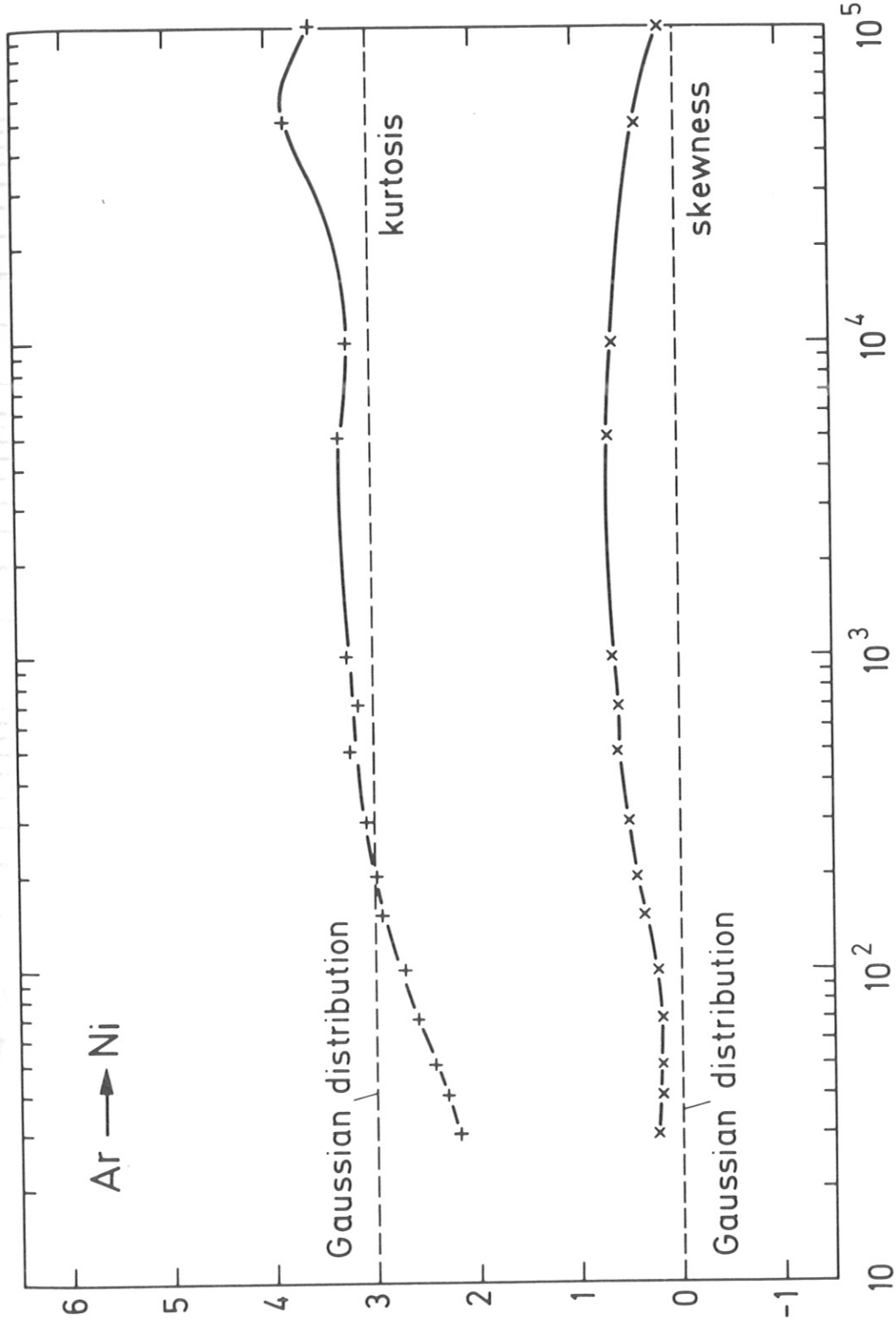

Fig. 24b The skewness (3. moment) and the kurtosis (4. moment of the depth distribution) versus the incident energy, E_0, are given for the bombardment of Ni with Ar at normal incidence.

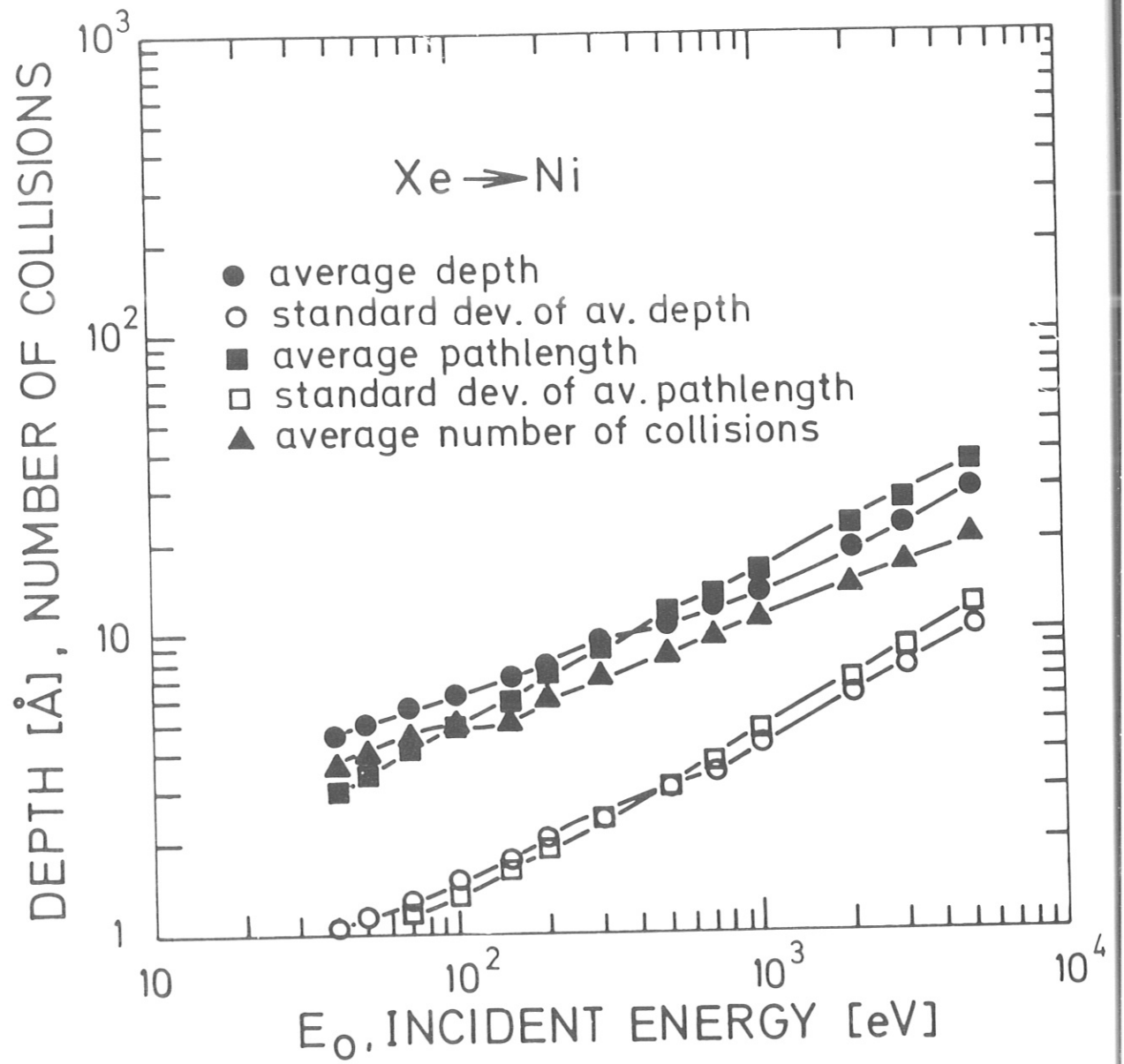

Fig. 25a The average depth (mean projected range or 1. moment) and the standard deviation of the average depth (2. moment), the average pathlength and the standard deviation of the average pathlength as well as the average number of collisions are given versus the incident energy, E_o, for the bombardment of Ni with Xe at normal incidence, $\alpha = 0^o$.

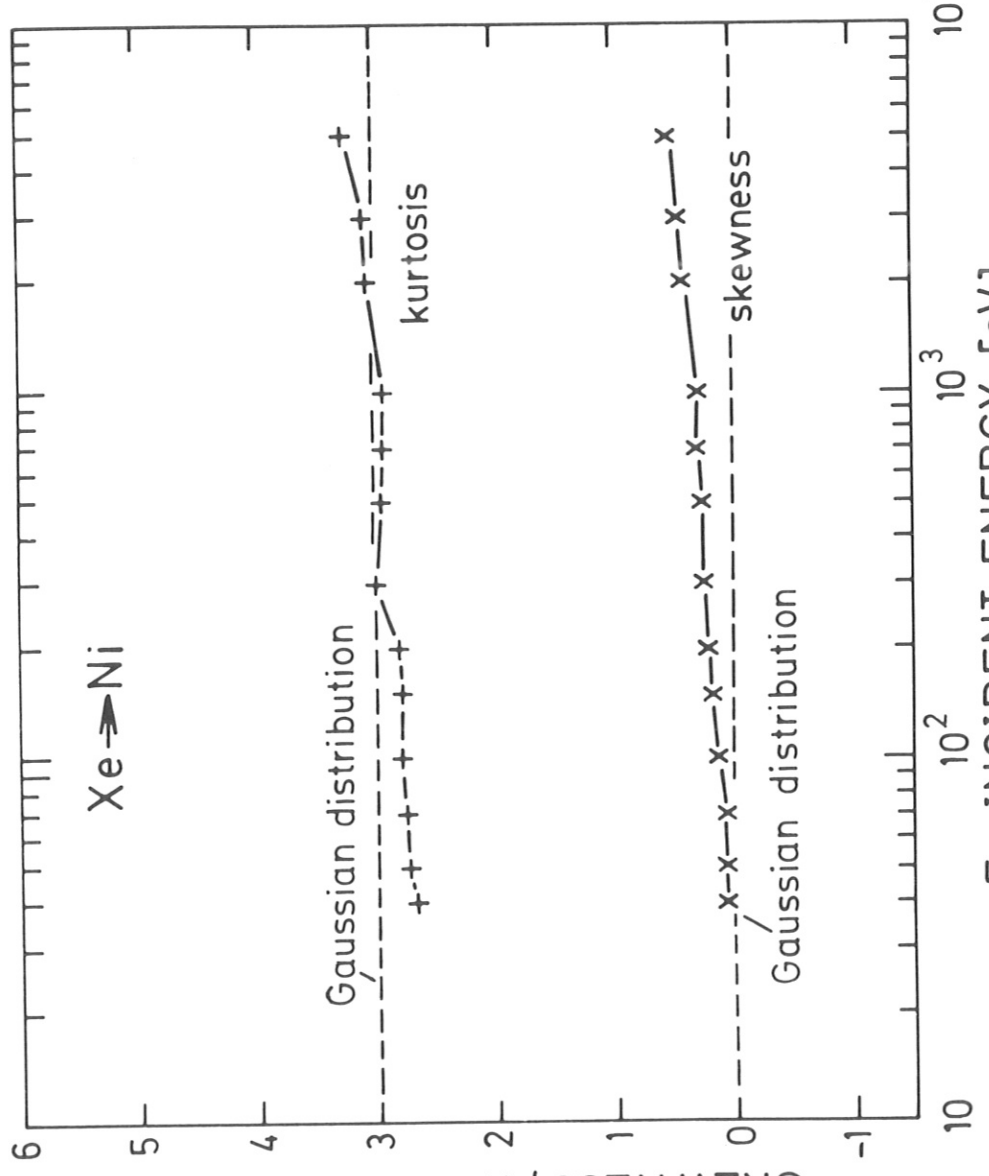

Fig. 25 b The skewness (3. moment) and the kurtosis (4. moment of the depth distribution) versus the incident energy, E_0, are given for the bombardment of Ni with Xe at normal incidence.

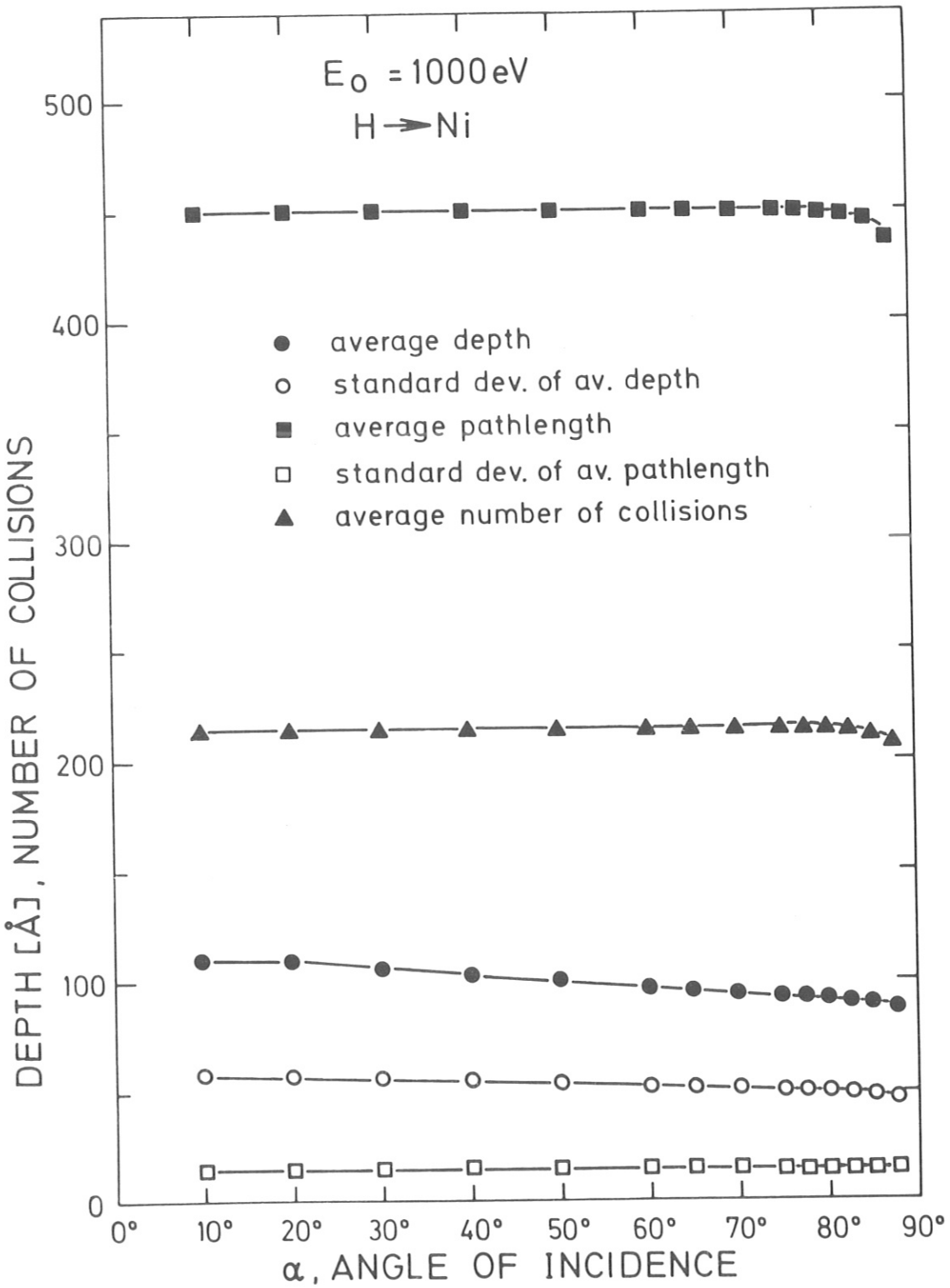

Fig. 26a The average depth (1. moment of the depth distribution) and the standard deviation of the average depth (2. moment), the average pathlength and the standard deviation of the average pathlength as well as the average number of collisions are given versus the angle of incidence, α, for the bombardment of Ni with H at an incident energy, E_o, = 1 keV.

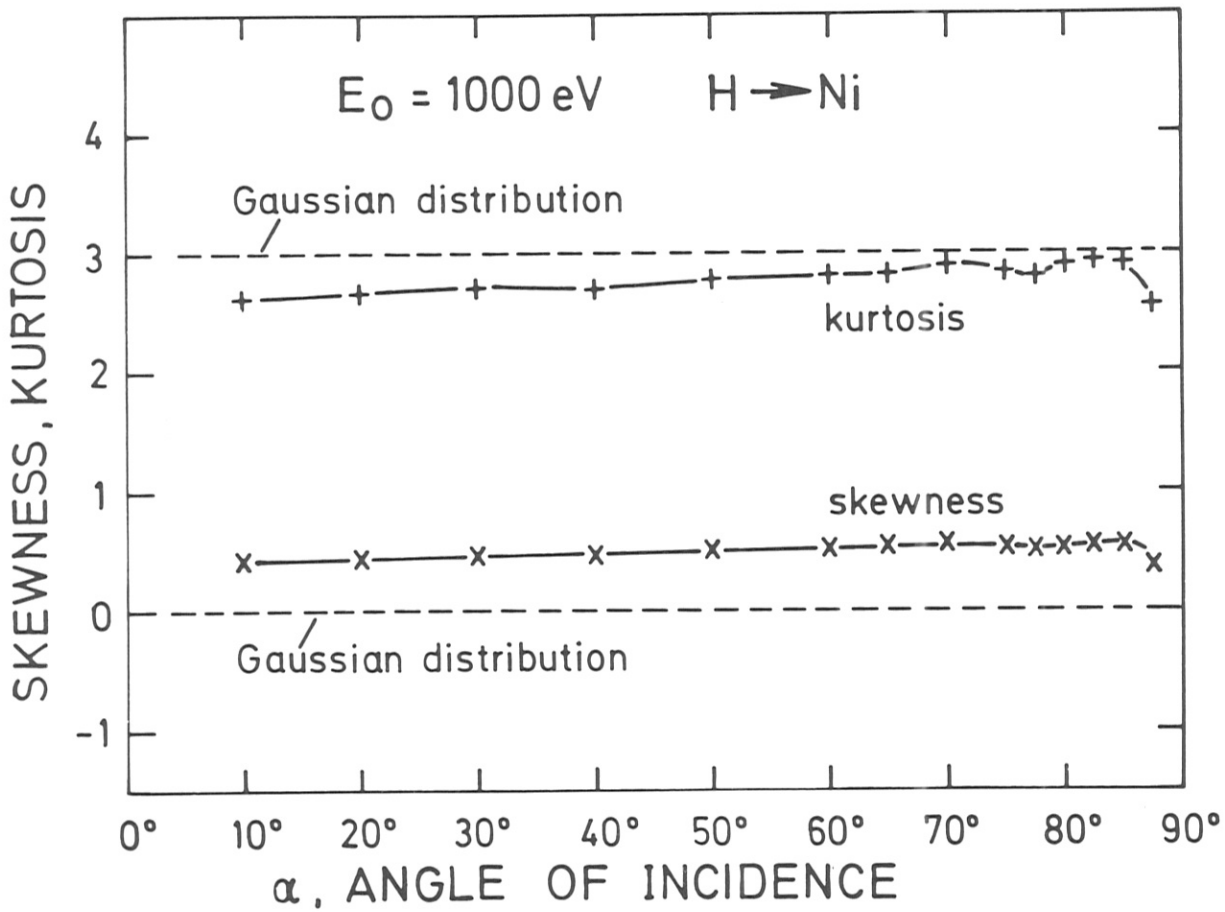

Fig. 26b The skewness (3. moment) and the kurtosis (4. moment) versus the angle of incidence, α , are given for the bombardment of Ni with H at an incident energy, E_o = 1 keV.

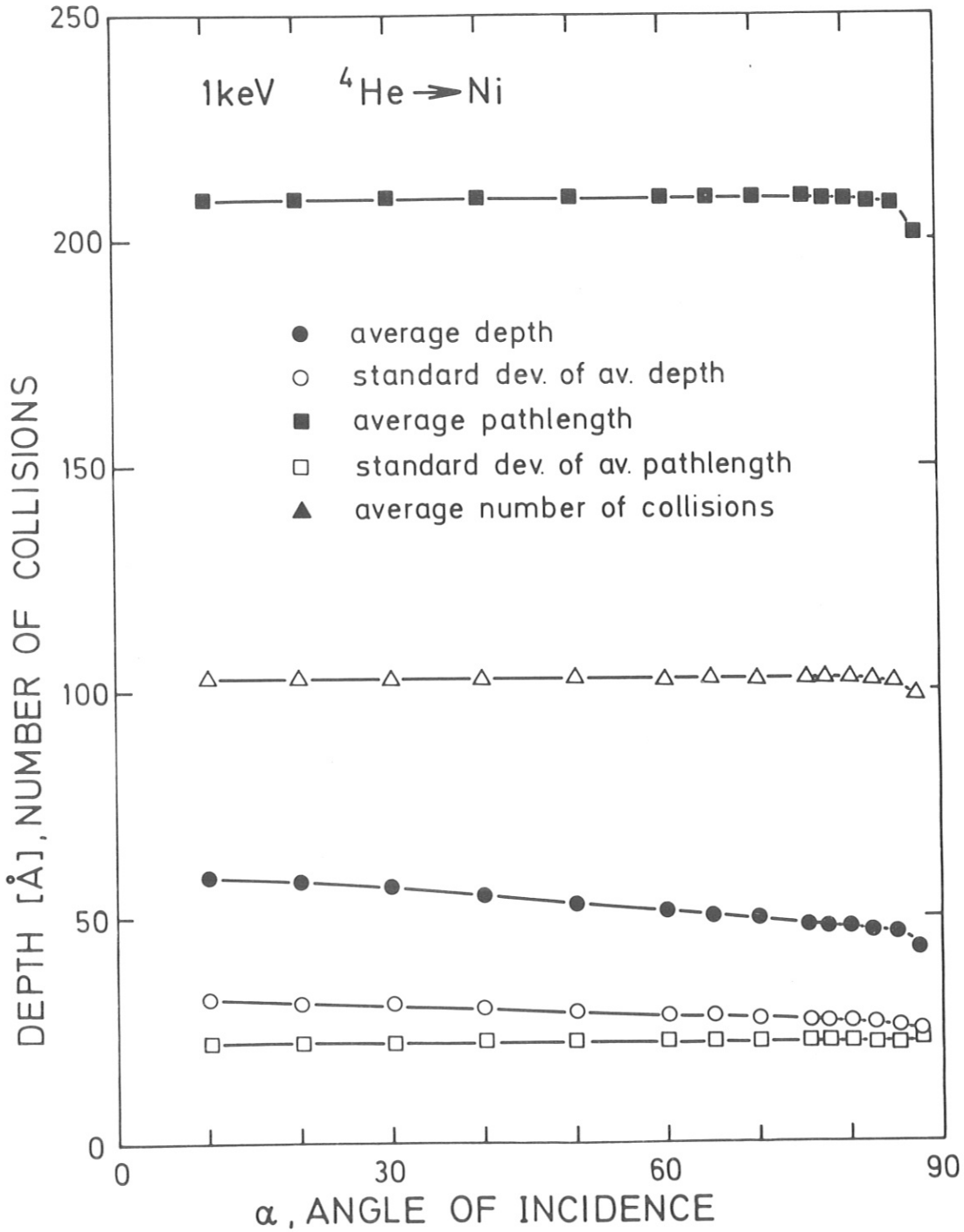

Fig. 27a The average depth (1. moment of the depth distribution) and the standard deviation of the average depth (2. moment), the average pathlength and the standard deviation of the average pathlength as well as the average number of collisions are given versus the angle of incidence, α , for the bombardment of Ni with ^4He at an incident energy, E_o = 1 keV.

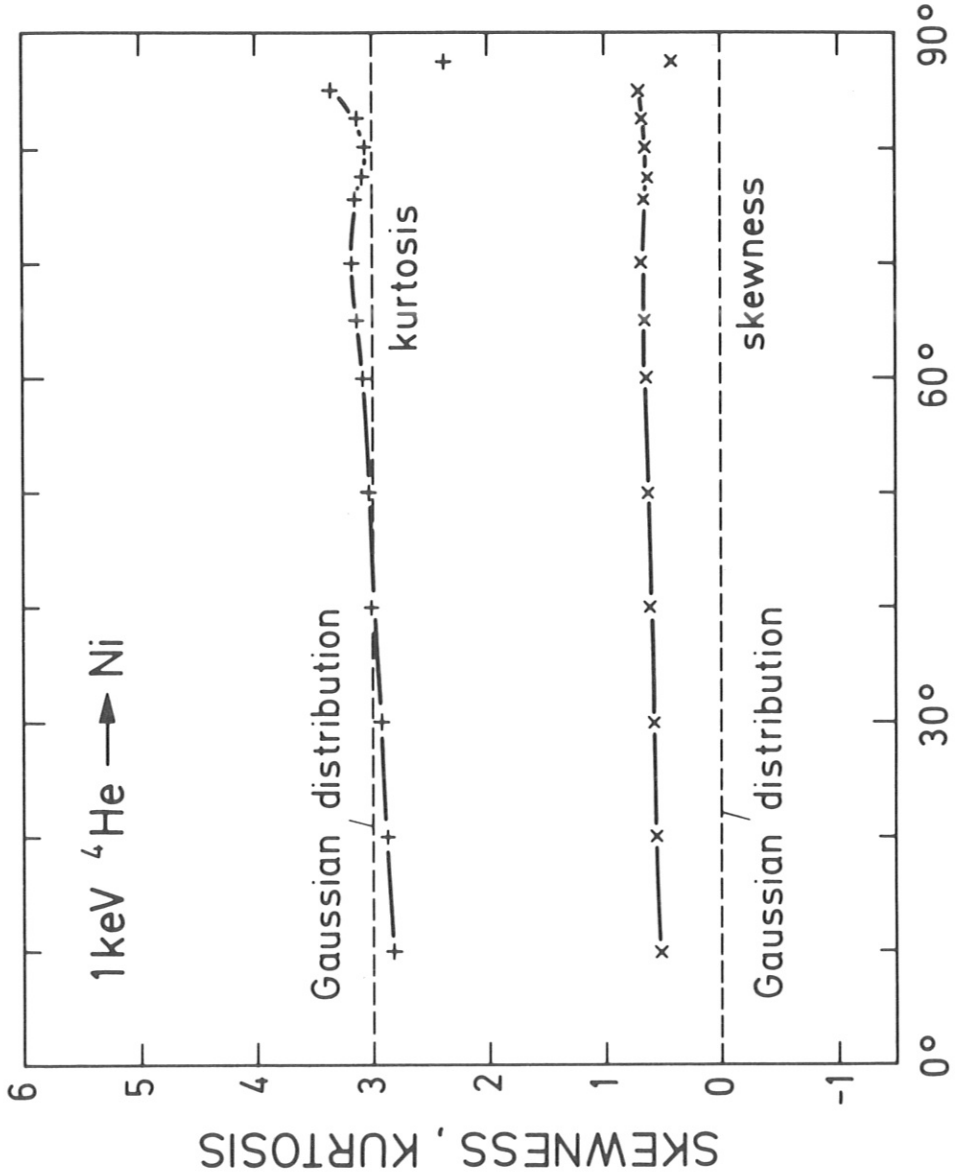

Fig. 27b The skewness (3. moment) and the kurtosis (4. moment) versus the angle of incidence, α , are given for the bombardment of Ni with ^{4}He at an incident angle, E_o = 1 keV.